The Molten Globule State of Maltose-Binding Protein: Structural Characterization by Electron Paramagnetic Resonance Spectroscopy

Vom Fachbereich Chemie der Universität Kaiserslautern

zur Verleihung des akademischen Grades

"Doktor der Naturwissenschaften"

genehmigte

DISSERTATION

(D386)

Vorgelegt von

Dipl.-Chem. Chen Nickolaus

Betreuer: Prof. Dr. Wolfgang E. Trommer

Datum der wissenschaftlichen Aussprache: 15.12.2016

This work was performed from May 2013 until October 2016 in the group of Prof. Dr. Wolfgang E. Trommer, Department of Chemistry, University of Technology Kaiserslautern, Germany.

Tag der wissenschaftlichen Aussprache: 15.12.2016

Promotionskommission:

Vorsitzender: Prof. Dr. Werner R. Thiel

1. Berichterstatter: Prof. Dr. Wolfgang E. Trommer

2. Berichterstatter: Prof. Dr. Antonio Pierik

For my family

欲穷千里目，更上一层楼。

-王之涣-

Enjoy a grander sight

by climbing to a greater height.

-Wang Zhihuan (Chinese poet)-

I. **INDEX**

II. LIST OF FIGURES

III. LIST OF TABLES

IV. ABBREVIATIONS

ANS	8-anilinonaphthalene-1-sulfonic acid
APS	ammonium persulfate
BCA	bicinchoninic acid
bp	base pairs
BSA	bovine serum albumin
CD	circular dichroism
CW	continuous wave
DEER	double electron-electron resonance
DHB	2,5-dihydroxybenzoic acid
DQC	double-quantum coherence
DQT	double-quantum transition
DTT	dithiothreitol
EI	electron ionization
EPR	electron paramagnetic resonance
FID	free induction decay
IPTG	isopropyl β-D-1-thiogalactopyranoside
ITC	isothermal titration calorimetry
MALDI-TOF MS	matrix-assisted laser desorption/ionization time-of-flight mass spectrometry
MBP	maltose-binding protein
MTS	(1-oxyl-2,2,5,5-tetramethyl-pyrroline-3-methyl) methanethiosulfonate
MTT	3-(4,5-dimethylthiazol-2-yl)-2,5-diphenyltetrazolium bromide
MWCO	molecular weight cutoff
NADPH	nicotinamide adenine dinucleotide phosphate, reduced form
NEB	New England Biolabs
NLSF	nonlinear least-squares data fitting

PCR	polymerase chain reaction
pI	isoelectric point
SDS-PAGE	sodium dodecyl sulfate polyacrylamide gel electrophoresis
SQC	single-quantum coherence
SQT	single-quantum transition
wt	wild type

V. FUNDAMENTAL CONSTANTS

molar gas constant	R	8.31451 J K^{-1} mol^{-1}
proton charge	e	$1.602177 \cdot 10^{-19}$ C
g-factor for free electron	g_e	2.0023193134
Planck constant	h	$6.62608 \cdot 10^{-34}$ J s
	$\hbar = \frac{h}{2\pi}$	$1.0545887 \cdot 10^{-34}$ J s
rest mass of electron	m_e	$9.10939 \cdot 10^{-31}$ kg
vacuum permeability	μ_0	$4\pi \cdot 10^{-7}$ m kg s^{-2} A^{-2}
Bohr magneton	μ_B	$9.284832 \cdot 10^{-24}$ J T^{-1}

VI. ZUSAMMENFASSUNG

Molten-Globule-Zustand des Maltose bindenden Proteins: Strukturelle Charakterisierung durch Elektronenspinresonanz-Spektroskopie

Wie Proteine sich innerhalb weniger Millisekunden korrekt falten können, ist eine der fundamentalen Fragen in der Biochemie. Ein beim Faltungsprozess durchlaufener Übergangszustand ist der *molten-globule*-Zustand (MG-Zustand), der sich unter bestimmten Bedingungen stabilisieren und untersuchen lässt. In diesem Zustand ähnelt die Sekundärstruktur dem nativen Zustand, während die Tertiärstruktur eher dem vollständig entfalteten Zustand entspricht. In dieser Arbeit wurde der MG-Zustand am Beispiel des Maltose bindenden Proteins (MBP) untersucht. Dazu wurde MBP bei pH 3,2 im MG-Zustand stabilisiert und dies mittels Fluoreszenz Spektroskopie bestätigt. Die Abstände zwischen definierten Aminosäuren im MG-Zustand wurden durch Spinlabels, die an gezielt mutierten Cysteinpaaren angebracht wurden, mittels Elektronenspinresonanz (EPR) gemessen und mit den Abständen derselben Aminosäuren im nativen Zustand verglichen. Anhand von sieben verschiedenen Doppelmutanten wurde die periphere Struktur mittels gepulster EPR analysiert, zwei weitere Doppelmutanten dienten dazu, die Struktur der molekularen Bindungstasche von MBP mittels CW-EPR zu untersuchen. Die Anwesenheit von Maltose führte im MG-Zustand zu einer deutlichen Veränderung der Abstände bestimmter Spinlabels in der peripheren Struktur. Dies deutet darauf hin, dass MBP Maltose sogar im MG-Zustand binden kann. Durch isotherme Titrationskalorimetrie (ITC) wurde diese Vermutung bestätigt: die Ergebnisse zeigen jedoch, dass der Bindungsprozess zwischen MBP und Maltose im MG-Zustand mit 11-fach geringerer Bindungsenthalpie erfolgt wie im nativen Zustand. Die Abstände der Spinlabel-Paare neben der Bindungstasche von MBP unterschieden sich im MG-Zustand vom nativen Zustand weder mit

noch ohne Maltose. Diese Ergebnisse weisen darauf hin, dass MBP im MG-Zustand rund um die Bindungstasche bereits eine klar ausgebildete Tertiärstruktur besitzt. Um diese Befunde zu bestätigen, sollten nun Untersuchungen anhand weiterer Doppelmutanten und mittels empfindlicherer Messungen wie z.B. DQC durchgeführt werden.

1. INTRODUCTION

Protein folding is a fundamental question in biochemistry. There is plenty of research about this topic and a key question must be answered, which is how a protein correctly folds within the millisecond timescale (Levinthal, 1969). Over the past two decades some researchers have tried to explain this process with a multidimensional landscape of energy, in which a protein folds through multiple routes and intermediate conformations (Wolynes et al., 1995). One of the thermodynamic stable intermediate states, the molten globule state, was first published by Dolgikh *et al*. (Dolgikh et al., 1981). They obtained this state through the moderate concentration of denaturant, acid pH, high temperature or removing the cofactor. Circular dichroism (CD) has revealed that proteins in the molten globule state possess a native-like secondary structure but a fluctuating tertiary structure. Nevertheless this intermediate is almost as compact as in the native state (Dolgikh et al., 1981). After that more and more research on the characterization of this state has been performed (Kataoka et al., 1997, Schwarzinger et al., 2008). The molten globule state can be monitored by fluorescence spectroscopy with the dye 8-anilinonaphthalene-1-sulfonic acid (ANS), which binds to the hydrophobic side chains of proteins and fluoresces (Mulqueen, Kronman, 1982, Semisotnov et al., 1991).

In this work the molten globule state of maltose-binding protein (MBP) was examined with electron paramagnetic resonance (EPR) spectroscopy. Mutationally created cysteine pairs in the double mutants MBP1 to MBP7 are distributed over the entire protein, which include the peripheral structure and imply long distances. For this purpose pulsed EPR was applied. The cysteine pairs in double mutants MBP8 and MBP12 are distributed near the binding pocket and can be investigated by CW EPR. In order to determine the binding affinity of MBP, an isothermal titration calorimetry (ITC) experiment was performed.

2. THEORETICAL BACKGROUND

2.1 Maltose-binding protein

Maltose-binding protein (MBP) has 370 amino acids, divided into two domains, which look like lobes. MBP forms a binding pocket for maltose or maltodextrin between these two domains, with a flexible hinge (Figure 1) (Spurlino et al., 1991).

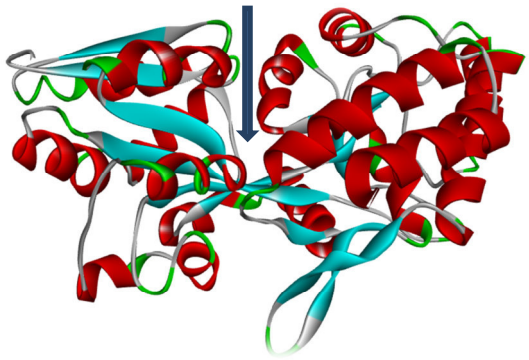

Figure 1. Illustration of MBP wild type (wt) with Discovery Studio Visualizer (PBD ID: 1anf)
α-Helix is colored red, β-sheet is cyan, β-turn is green, and random coil is gray. The arrow indicates the binding pocket.

MBP binds to its ligand in the periplasmic space and delivers it via the membrane-bound $MalFGK_2$ complex to the cytoplasm (Figure 2).

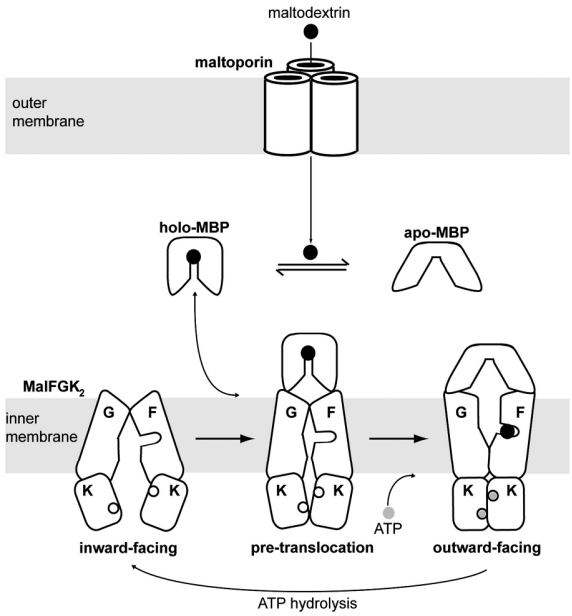

Figure 2. Schematic illustration of the uptake of maltodextrin into the cytoplasm of *E. coli* (Oldham et al., 2013)

Maltodextrin diffuses into the periplasmic space through maltoporin and then is bound to MBP. Liganded MBP binds to the $MalFGK_2$ complex of the inner membrane. After binding of ATP to $MalFGK_2$, maltodextrin is released from MBP and binds to the $MalFGK_2$ complex through a conformational change of the latter. After hydrolysis of ATP, MBP is released to the periplasmic space, and maltodextrin is released into the cytoplasm.

As a candidate for structural research, MBP has its advantages: it is a moderately large protein, which has only one peptide chain (Spurlino et al., 1991); its wild type does not contain free cysteine residues and disulfide bonds (Sheshadri et al., 1999); it is thermally stable (Ganesh et al., 1997); it is well investigated in its native state. Crystallographically determined structures here are reported at 2.3 Å resolution (Spurlino et al., 1991). Sheshadri *et al*. have found out that MBP can be stabilized in its molten globule state at pH 3.0 (Sheshadri et al., 1999).

2.2 Electron paramagnetic resonance and spin labeling

Electron paramagnetic resonance (EPR) spectroscopy is a powerful tool to investigate biological structures, such as iron-sulfur clusters (Roessler et al., 2010) and proteins, into which spin labels have been introduced (Hubbell, Altenbach, 1994). It is commonly used to study the environment of a radical center, or the distance between two radicals. Continuous wave (CW) EPR is a suitable method to determine the distance between a radical pair from 0.8 to 1.5 nm (Banham et al., 2008), while double electron-electron resonance (DEER) EPR is proper for long-distance determination up to 10 nm (Jeschke, 2012). In addition to the DEER EPR, double-quantum coherence (DQC) EPR has additional advantages: it yields stronger signals due to the non-selective pulses and it suppresses the proton modulation due to the six-pulse sequence (Borbat, Freed, 1999).

EPR is a technique based on the resonance between unpaired electrons and an electromagnetic wave in a magnetic field. An electron has only one spin quantum number $S = 1/2$. In the presence of a magnetic field B_0, the degenerate energy level splits into two levels: a lower energy level with the magnetic spin quantum number $m_s = -1/2$ (antiparallel to the magnetic field), and a upper energy lever with $m_s = +1/2$ (parallel to the magnetic field). Electrons distribute themselves to the two energy levels according to the Boltzmann distribution law. Electrons from the lower energy level will be excited to the upper energy level by changing the frequency of the radiation until the resonance condition occurs (equation (2.2-1)) (Wedler, 1997) (Figure 3).

$$\Delta E = h\nu = g_e \mu_B B_0 \qquad (2.2\text{-}1)$$

ΔE: energy difference between the lower and upper energy levels

h: Planck constant

ν: resonance frequency

g_e: g-factor for free electron

μ_B: Bohr magneton

B_0: external magnetic field strength

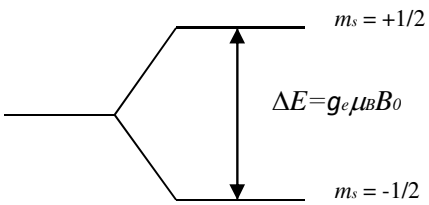

Figure 3. Schematic illustration of the splitting of a degenerate energy level of an electron, and the allowed transitions (Berliner, 1976) (modified)

This single transition leads to a one-line-spectrum. In practice, the resonance condition will be fulfilled by changing the external magnetic field, while the frequency of the radiation stays constant. The most commonly used magnetic field strength in X-band spectrometers is around 0.34 T, which corresponds to 9.5 GHz calculated with equation (2.2-1). This falls in the microwave range. (Wedler, 1997)

2.2.1 Hyperfine coupling

Except the electron spin, there is also nuclear spin, which has mostly interaction with electron spins. This leads to a further splitting of the energy levels. A nitroxide radical is taken as an

example, and the energy levels and the allowed transitions are illustrated in Figure 4. (Wertz, Bolton, 1986)

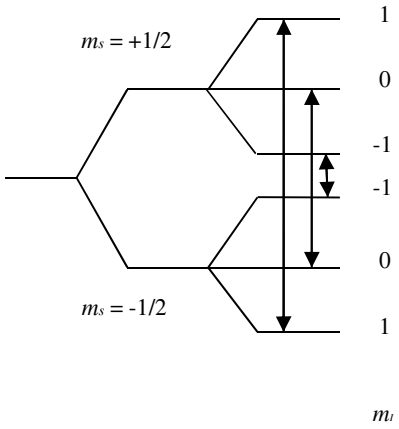

Figure 4. Schematic illustration of the hyperfine structure of a nitroxide radical (Wertz, Bolton, 1986)

The nitrogen atom ^{14}N has a nuclear spin quantum number $I = 1$, thus there are three magnetic spin quantum numbers S: -1, 0, and 1. Each level with regard to the electron spin, splits further into three levels. According to the selection rules, there are only three transitions allowed, which are between the same nuclear spin quantum number (Wertz, Bolton, 1986). This leads to a three-line-spectrum, which is typical for ^{14}N (Figure 5).

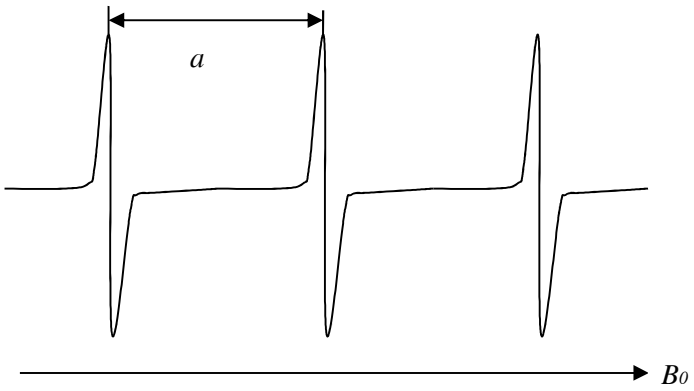

Figure 5. Sketch of a CW spectrum of free nitroxide radicals

Beside the external magnetic field B_0, the magnetic field of a nuclear spin affects the electron spin as well (Wedler, 1997). The local magnetic field is given by

$$B_{loc} = B_0 + am_I \qquad (2.2.1\text{-}1)$$

B_{loc}: local magnetic field strength of electron spin

B_0: external magnetic field strength

a: hyperfine structure constant

m_I: magnetic nuclear spin quantum number

Putting the equation (2.2.1-1) into equation (2.2-1) gives

$$h\nu = g\mu_B(B_0 + am_I) \qquad (2.2.1\text{-}2)$$

g is g-factor, which depends on the environment of the electron.

2.2.2 CW EPR

One of the applications of EPR spectroscopy is to determine the distance between two radicals. This is based on the dipole-dipole interaction between these two spins. They are named as spin A and spin B with the magnetic moment $\overrightarrow{m_A}$ and $\overrightarrow{m_B}$, respectively. The distance between the two spins is *r*. The energy due to the dipole-dipole interaction is

$$E = \frac{\overrightarrow{m_A} \times \overrightarrow{m_B}}{r^3} \qquad (2.2.2\text{-}1)$$

In the presence of an external magnetic field, the formula is simplified as follows

$$E_{dipole} = \frac{m_A m_B}{r^3}(1 - 3\cos^3\theta) \qquad (2.2.2\text{-}2)$$

θ is the angle between the external magnetic field and the axis through spin A and spin B (Figure 6).

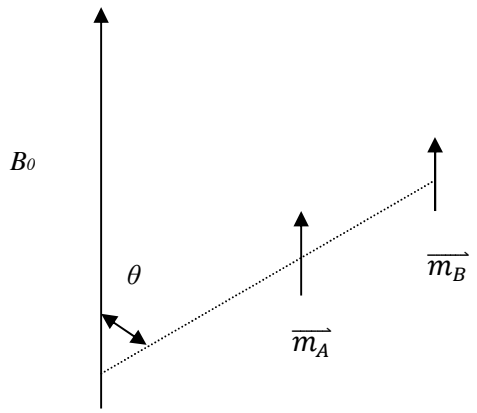

Figure 6. Dipole-dipole interaction between spin A and spin B in the presence of an external magnetic field B_0 (Weil et al., 1994) (modified)

The formula reveals that the dipole-dipole interaction is inversely proportional to the cubic of the distance between the two spins (Berliner, 2000). With the CW technique, spectra can be recorded easily and quickly, but its application due to the broadening of spectra caused by dipole-dipole interactions, is limited to a maximum distance of 2.5 nm between two spins (Rabenstein, Shin, 1995).

2.2.3 Spin relaxation

As mentioned before, electrons are excited from a lower energy level to an upper energy level by absorbing energy, e.g. from microwaves. At the same time electrons from the upper energy level return to the lower energy level, which is a first-order reaction. The time needed to return is called spin-lattice relaxation time, T_1, also called longitudinal relaxation time. In contrast, there is a spin-spin relaxation time, T_2, at which the magnetization of electrons in the same energy level reaches the equilibrium, also called transverse relaxation time (Wertz, Bolton, 1986). According to the Heisenberg's uncertainty principle

$$\Delta E \Delta t \geq \frac{h}{2\pi} \qquad (2.2.3\text{-}1)$$

Assuming that Δt is T_2, ΔE increases with decreasing T_2, leading to a broadening of spectra (Wertz, Bolton, 1986).

2.2.4 Pulsed EPR

In contrast to the CW technique, pulsed EPR utilizes electron-electron coupling to determine the distance between the spins (Berliner, 2000). The electron-electron coupling frequency is given by

$$\omega_{ee} = \omega_{dd}(3\cos^2\theta - 1) + J = \frac{g_A g_B \mu_B^2 \mu_0}{4\pi\hbar}\frac{1}{r^3}(3\cos^2\theta - 1) + J \qquad (2.2.4\text{-}1)$$

ω_{ee}: electron-electron coupling frequency

ω_{dd}: dipole-dipole interaction frequency

θ: angle between the external magnetic field and the axis through these dipoles

J: exchange coupling (isotropic)

g_A or g_B: g-factor of spin A or spin B

μ_B: Bohr magneton

μ_0: vacuum permeability

$\hbar$: reduced Planck constant

r: distance between spin A and spin B

The electron-electron coupling depends on the distance r and the angle θ. In the presence of the external magnetic field, the two spins stay parallel to each other, but the angle θ is random. However, if the frequency ω_{ee} is plotted against the angle θ, it becomes apparent the greatest possible angle is 90° (Jeschke, 2012) (Figure 7).

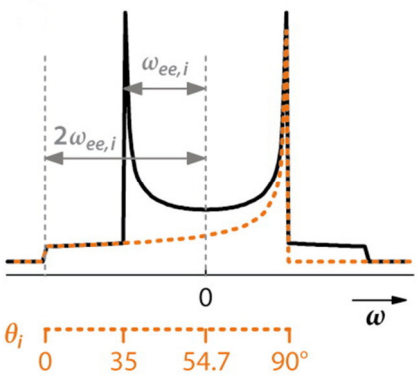

Figure 7. Pake pattern of two dipoles (Jeschke, 2012)
The frequency ω_{ee} depends on the angle θ (dashed line). The angle scale is for one dipole illustrated. At an angle of 90° there is a maximum of the signal, while at an angle of 35° there is a minimum.

One problem of the CW technique is to separate dipole-dipole interaction from other interactions, which can occur if the two spins are localized too close together. If the distance between the two spins is far enough, e.g. at least 1 nm, there is still a dipole-dipole interaction but also an unwanted exchange coupling. However, if the spins are not delocalized, the exchange coupling is isotropic and the effect on the spectra can be neglected (Steinhoff et al., 1997). If the distance is larger than 2 nm, the exchange coupling is negligible in general (Berliner, 2000). Under these conditions, the formula (2.2.4-1) can be rewritten as

$$r = \left(\frac{52{,}041\ MHz}{\omega_{ee}(90°)}\right)^{1/3}\ \text{nm} \qquad (2.2.4\text{-}2)$$

If it is possible to determine the frequency difference between the two peaks of the Pake pattern (see Figure 7), it is possible to calculate the distance between the two dipoles (Berliner, 2000). Thus, pulsed EPR is suitable to determine distances between 1.5 and 8 nm (Pannier et al., 2011).

2.2.5 Hahn echo

To understand the pulsed technique, it is necessary to introduce the Hahn echo (Hahn, 1950) at first. It is assumed that the orientation of the external magnetic field is along the z-axis. Additionally a π/2 pulse is then applied to the x-axis, in order to tip the net magnetization of spins from the z-axis to the –y-axis. Due to the inhomogeneity of spins, they fan out in the xy-plane with different velocity (dephasing). If a π pulse is applied in the time τ_1 after the π/2 pulse, the magnetization of spins turns 180° to the +y-axis, without changing the direction of motion and velocity of spins, meaning that the spins refocus and lead to a maximal magnetization in the time τ_1 (Figure 8). This refocused signal at the end is the Hahn echo.

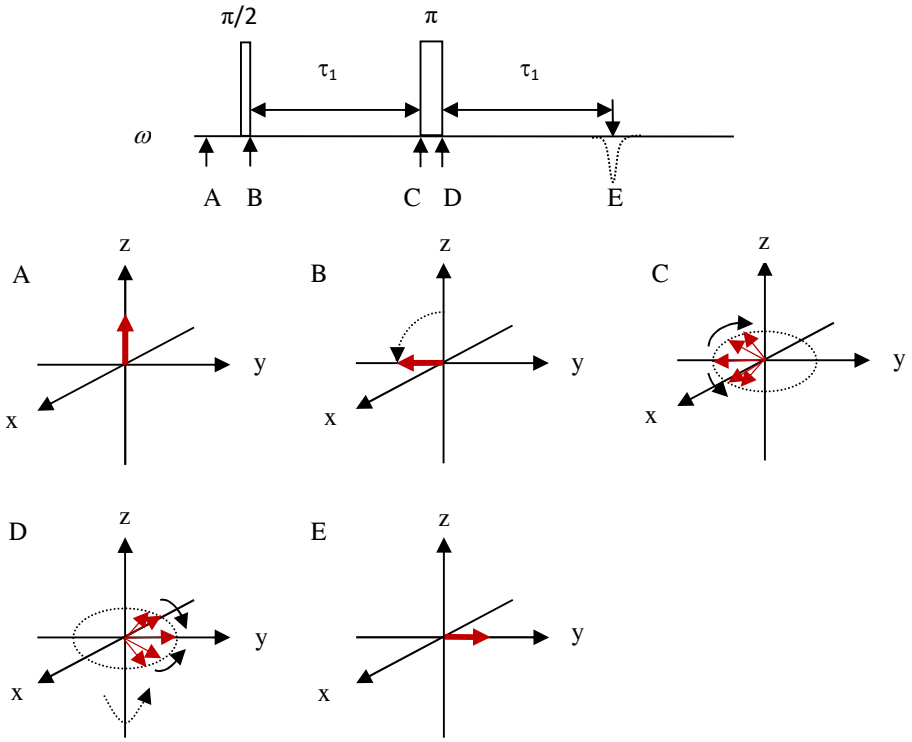

Figure 8. Schematic illustration of the net magnetization of spins in the course of the combination of different pulses (Junk, 2012) (modified)

Spins tipped into the xy-plane will turn back to the z-axis in the time T_1, which is mentioned before as spin-lattice relaxation time. The contribution of net magnetization of spins keeps a maximum right after the tipping from the z-axis to the xy-plane, and decreases with the time T_2, until at equilibrium. T_2 is identical with the spin-spin relaxation time (Wedler, 1997). This process is called free induction decay (FID) and is caused by the interaction between the individual spins, such as flip-flops. The inhomogeneity of spins is caused by the different local magnetic field (Hahn, 1950), which can be used to investigate the local structures. If the spins stayed in the xy-plane, there would be no signal any more after the equilibrium had been reached. Therefore, T_1 ensures that the spins turn back to the z-axis, so that they can be tipped to the xy-plane repeatedly.

2.2.6 Four-pulse DEER

Hahn echo is a valuable technique; however, its use is limited due to the dead time. In order to resolve this problem, a second microwave source with different frequency is applied. In a four-pulse DEER experiment, spins are divided into 2 groups, spins A and B. A frequency termed observe-frequency (ω_{obs}) affects spins A, while the other frequency termed pump-frequency (ω_{pump}) affects spins B (Pannier et al., 2011) (Figure 9).

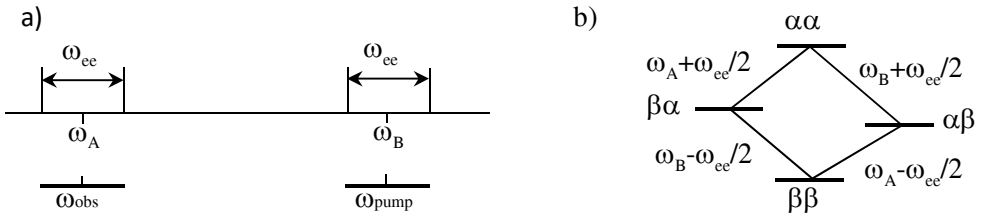

Figure 9. a) Schematic spectrum of spin A and spin B excited by observe-frequency and pump-frequency, respectively. b) Energy level diagram of the spin pairs (Jeschke, 2002)

The ω_{obs} and ω_{pump} should be separated far enough from each other, so that the excitation bandwidths will not overlap. The dipole-dipole interaction between the spin pairs results in a splitting of transitions of spin A and spin B, respectively. The change of magnetization of spin B results in the change of local magnetic field at spin A, which can be recorded as echo and analyzed for dipole-dipole interaction (Jeschke, 2002). The sequence of pulses for the four-pulse DEER experiment is illustrated in Figure 10.

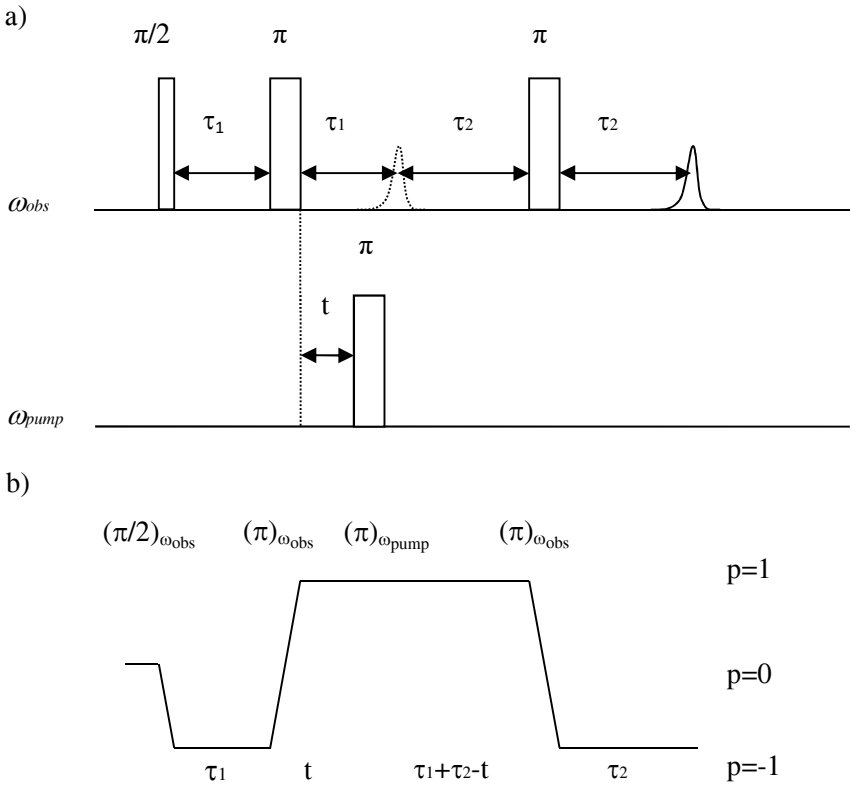

Figure 10. a) Schematic illustration of pulse combination and b) coherence pathway of a four-pulse DEER experiment (Pannier et al., 2011) (modified)

On the observe-frequency side, the dotted signal is an undetectable Hahn echo described before. During the time τ_1 between the second pulse and the Hahn echo on the observe-frequency side,

another π pulse on the pump-frequency side is applied, in order to invert spins B, which results in a change of local magnetic field at spins A. This leads to a perturbation of formation of the original Hahn echo, instead, spins A dephase again. After the fourth pulse, spins A refocus again, which can be recorded as signals. This process can also be illustrated in coherence pathway (Figure 10 b)). Varying the position of the third pulse on the time scale, the intensity of signals varies (Pannier et al., 2011). This time domain signal can be translated into the Pake pattern by Fourier transformation (Figure 11).

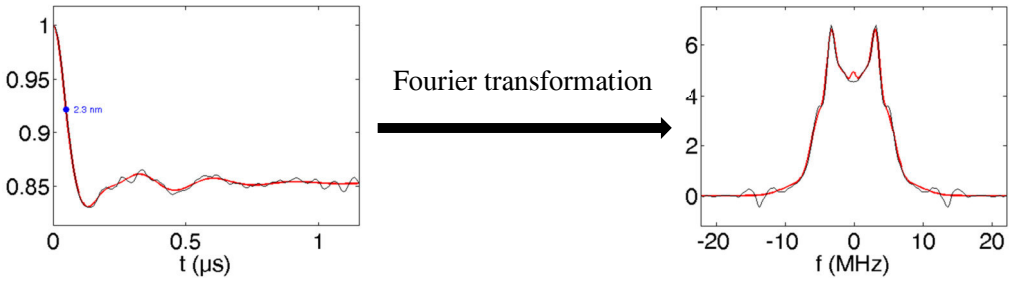

Figure 11. The time domain signals (left) are translated into a Pake pattern (right) by Fourier transformation.

2.2.7 DQC

As mentioned before, the pulsed EPR detects the spin echo signals to analyze the electron spin interactions. In the thermal equilibrium, a density matrix of a quantum system contains only diagonal elements, which correspond to the energy levels. The off-diagonal density matrix elements are zero in the thermal equilibrium. By using certain pulses to disrupt the thermal equilibrium, the off-diagonal elements with distinct phases (coherence) can be detected as echo of interest, until the system reaches its thermal equilibrium again. Only the single-quantum coherence (SQC) is detectable (Figure 12) (Borbat, Freed, 2013).

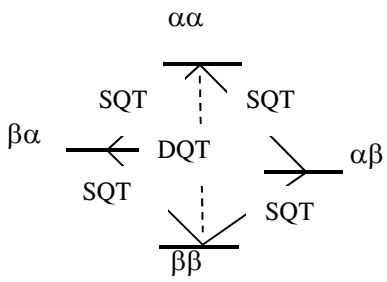

Figure 12. Energy level diagram of the spin pairs (Borbat, Freed, 2013) (modified)

SQT means single-quantum transition, while DQT means double-quantum transition. The pulse combination is aimed to convert the DQC to detectable in-phase SQC (Figure 13).

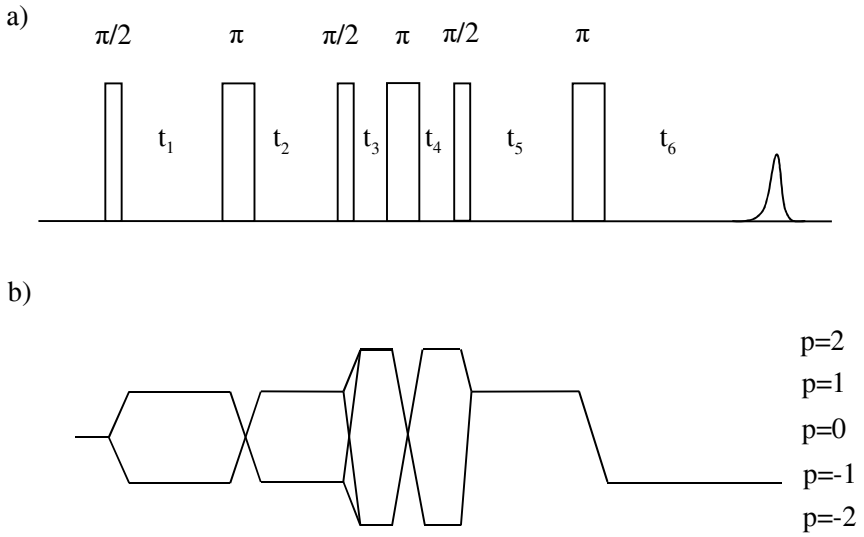

Figure 13. a) The sequence of pulses and b) the coherence pathway of a 6-pulse DQC experiment (Borbat, Freed, 1999)

2.2.8 Site-directed spin labeling

The presence of an unpaired electron is a prior condition for EPR measurement. However, not every biological molecule contains radicals, or transition metals. Site-directed spin labeling extends the range of application of EPR. Spin labeling, as its name suggests, introduces a spin label into the investigated system, such as protein (Berliner, 1976). On the other hand, such a protein should contain an anchor group (often cysteine) for the spin label. The most commonly used spin label is (1-oxyl-2,2,5,5-tetramethyl-pyrroline-3-methyl) methanethiosulfonate (MTS) (Figure 14).

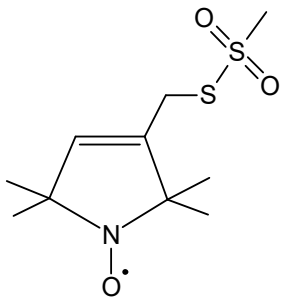

Figure 14. Structural formula of MTS

The bivalent sulfur atom of MTS reacts with the cysteine residue (Figure 15), hence, is attached to proteins via a covalent bond (Berliner, 1989). Site-directed mutagenesis allows the mutation of an amino acid into cysteine on demand. With these two techniques, we can introduce two MTS targeted into proteins, so that the distance between them can be determined.

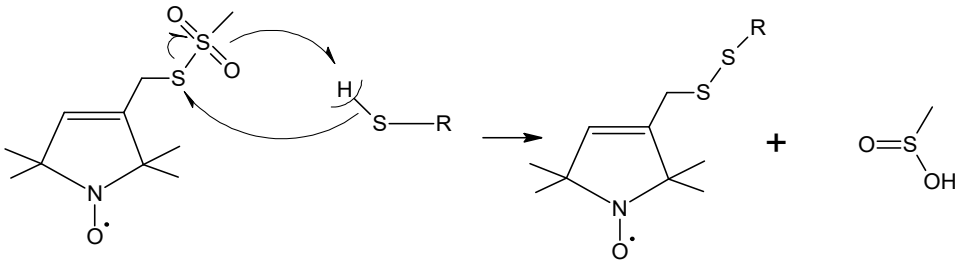

Figure 15. Reaction scheme of MTS reacting with the cysteine residue

The thiol group of cysteine is deprotonated at pH 6.7, thus is able for nucleophilic attack on the thio-sulfur of the thiosulfonate, which results an electron pair transfer from the peripheral to the central sulfur atom of the thiosulfonate. Consequently, the oxygen atom of the formed sulfinate ion attacks a proton to form a stable structure sulfinic acid. At the end MTS is bound to a protein via a disulfide bond and a methanesulfinic acid is split.

2.3 ITC

ITC is a calorimetric method to determine the thermodynamic characteristics of a chemical reaction, which occurs when two components are mixed. One component A will be added drop by drop to the reaction cell containing the other component B (Figure 16). The generated enthalpy changes are compensated by the device power in order to maintain the isothermal condition, which is fulfilled by measuring and minimizing the temperature difference between the reaction and the reference cells. During addition of A, the concentration of the free component B decreases until it is saturated, so that the magnitude of peaks decreases until it stays similar at low level due to e.g. dilution effect (Leavitt, Freire, 2001).

$$A + B \rightleftharpoons AB$$

Figure 16. Schematic representation of a binding process of two components

The binding affinity constant K_a in the equilibrium is calculated as below:

$$K_a = \frac{[AB]}{[A][B]} \tag{2.3-1}$$

$[AB]$: concentration of complex AB in the equilibrium

$[A]$ or $[B]$: concentration of component A or B, respectively, in the equilibrium

Using the measured binding affinity constant K_a and the enthalpy change $\Delta H°$, together with the absolute temperature T, the Gibbs energy change $\Delta G°$ and the entropy change $\Delta S°$ can be calculated as below:

$$\Delta G° = -RT \ln K_a = \Delta H° - T\Delta S° \tag{2.3-2}$$

ΔG: Gibbs energy change

R: gas constant

T: absolute temperature

$\Delta H°$: enthalpy change

$\Delta S°$: entropy change

If the measurements are carried out at different temperatures, the heat capacity $\Delta C_p°$ can be calculated, as well (Leavitt, Freire, 2001):

$$\Delta C_p° = \frac{\partial \Delta H}{\partial T} \tag{2.3-3}$$

Furthermore, using ITC the number of binding sites can also be determined (Hellmann et al., 2001).

2.4 Nonlinear least-squares fitting (NLSF)

After the correct collecting of experimental data, an appropriate analysis of the data is important as well. One of the most commonly used methods for the analysis in biochemistry is nonlinear least-squares fitting (NLSF) (Johnson, 1992). The experimental data consist of an independent variable (x) and a dependent variable (y). The aim of the fitting is to find out the relationship between x and y, so called a fitting function (Kemmer, Keller, 2010). We assume the set of experimental data as x_i y_i, the fitting data as x_i $f(x_i)$, the weighting factor of the ith data point as w_i, so the sum of squared residuals (SSR) is given by:

$$SSR = \sum_i w_i(y_i - f(x_i))^2 \qquad (2.4\text{-}1)$$

For an unweighted fitting, w_i equals 1.

By changing the parameters of the function $f(x)$, the difference between $f(x_i)$ and y_i varies. To decide which combination of parameters results in the best fit is to find out when SSR is minimum. If the function is linear in the parameters, such fitting is linear least-squares fitting. By analogy, if the function is nonlinear in the parameters, this fitting is nonlinear least-squares fitting (Kemmer, Keller, 2010).

After a brief introduction about NLSF, the limitation of the application of NLSF should also be mentioned. In order to use NLSF as an analysis method, the following assumptions must be valid: the independent variables are free of experimental uncertainty; the dependent variables exhibit the experimental uncertainty like a Gaussian distribution with a mean of zero; the

individual data must be independent of one another; sufficient data points must be collected in order to give good random experimental uncertainties. If the assumptions above are not valid, NLSF should be applied carefully (Johnson, 1992).

In this work, the fittings of the far-UV-CD data with Solver (Microsoft Excel) (Kemmer, Keller, 2010), ITC data with SEDPHAT (Schuck, 2000), DEER data with DeerAnalysis (Jeschke et al., 2006) and CW data with DIPFIT (Steinhoff et al., 1997) are all based on NLSF.

After finding out the combination of parameters for the best fit, another question should be answered: how confident the results of NLSF are. The utilized software above all contains functions based on e.g. χ^2 test or F test to compute the confidence intervals. The Fisher's F distribution is available only for linear fitting. The variance of SSR within a certain threshold is observed by changing one of the parameters away from its best-fit value. The value of this parameter, with which SSR gives the threshold value, can be used to determine the confidence constraint. Some nonlinear fitting can be treated as linear approximately for small variance from the best fit value, if the SSR variances meet the parabola form with the best fit value as minimum (Kemmer, Keller, 2010).

3. METHODS

3.1 Gene technology

All implementation of gene techniques is in sterile condition.

3.1.1 Site-directed mutagenesis

Mutagenesis involves the modification of DNA molecules, such as substitution, deletion and insertion of a single base pair or of sequences. Principally two primers are required which contain the desirable modifications (Berg et al., 2011). In this work the protocol of Zheng *et al*. was a guideline of primer designs for substitution. The pair of primers should overlap partially and both should contain the mutations (Figure 17). The overlap area includes about 20 base pairs (bp) and at least 8 bp should be left at the 3' end. It is suggested to introduce a silent mutation as a new cutting site for a restriction enzyme, so that an identification of the successful mutants by digesting with the restriction enzyme is possible. At least one G or C should exist at the 3' end of both primers, so that the primers adhere to the template more tightly because of the 3 hydrogen bonds between G and C (Zheng et al., 2004).

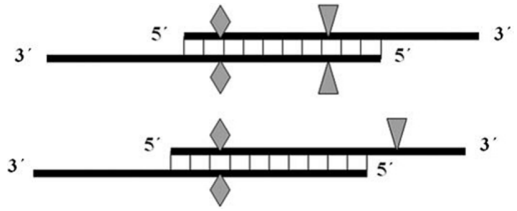

Figure 17. Schematic representation of primer designs (Zheng et al., 2004)
The desirable mutations are shown as diamond, which should be contained in both primers, while the silent mutations are shown as triangle, which can be contained in one strand of the primer pair or in both of them.

The primer pairs used in this work are listed in Table 1.

Table 1. Summary of the primer pairs used in this work

Primer	Sequence (5'→3')	Description
MC298Pfor	AAAGACAAACCGCTGGGTGCCGTAGCGCTGAAG	Mutation from MBP6 to MBPwt
MC298Prev	GCACCCAGCGGTTTGTCTTTATTAACCGCTTCC	
MC325Qfor	CGCCCAGAAAGGTGAAATCATGCCGAACATCCC	
MC325Qrev	TGATTTCACCTTTCTGGGCGTTTTCCATGGTGG	
MG13Cfor	CATATGGATTAACTGCGATAAAGGCTATAACGG	Mutation from MBPwt to MBP12
MG13Crev	TCGCAGTTAATCCATATGACCAGTTTACCTTC	
MT237Cfor	CAACATCGACTGCAGCAAAGTGAATTATGGTG	
MT237Crev	ACTTTGCTGCAGTCGATGTTGGACCATGCCCAC	
M13for (-20)	GTAAAACGACGGCCAGT	For sequencing
M13rev (-48)	AGCGGATAACAATTTCACACAGGA	

The plasmids of MBP1 to MBP7 were kindly provided by Professor Raghavan Varadarajan, Molecular Biophysics Unit, Indian Institute of Science, Bangalore, India. The vector pMALp2 was used for cloning of the gene *MalE* to the template pMALp2MBP, which has an ampicillin resistance. The mutations in MBP8 were introduced by my colleague Benjamin Selmke. In order to produce the new double mutant MBP12, the plasmid of MBP6 was chosen to be mutated to MBPwt, and further to MBP12. The information about the positions of all mutated amino acids is given in the appendix.

The DNA sequence with the desirable mutations was amplified by the polymerase chain reaction (PCR). The procedure is based on the protocol of (Wang, Malcolm, 1999) and the use of the Phusion HF DNA polymerase of New England Biolabs (NEB).

After PCR the parental DNA was digested with the restriction enzyme DpnI. This mixture was purified with the NucleoSpin® Gel and PCR Clean-up kit (Macherey-Nagel) and transformed into competent cells.

3.1.2 Transformation

The modified plasmid can be transformed to competent bacterial cells in laboratory, in order to amplify a plasmid or to express a protein.

5 ng plasmid DNA or the complete mixture after the purification with the NucleoSpin® Gel and PCR Clean-up kit were added to 100 µl of competent *E. coli* and incubated for 10 minutes on ice. After heat shock at 42 °C for 90 seconds, the mixture was put on ice immediately for another 2 minutes. 1 ml of LB medium without antibiotics was added to the mixture which then was incubated at 37 °C for 40 minutes by shaking (850 rpm with Thermomixer comfort, Eppendorf). After centrifugation for 5 minutes, 950 µl of liquid were removed. The cells were resuspended in the rest of the liquid and transferred to an LB-Amp-Agar petri dish. The dish was incubated at 37 °C for about 16 hours, until clones were visible.

3.1.3 Plasmid isolation

For plasmid amplifying, the NEB5α competent *E. coli* was used. After transformation of plasmid, one clone was transferred to 6 ml of LB medium, and cultivated at 37 °C for 16 hours. Cells were harvested and the plasmid was isolated with the NucleoSpin® Plasmid kit (Macherey-Nagel) according to the enclosed protocol.

3.1.4 Cell culture

For expressing proteins, the BL21 (DE3) competent *E. coli* was used. After transformation, cells were cultivated in TB medium at 37 °C by shaking (200 rpm with Thermo Scientific, MaxQ 400), until OD_{600} reached 1.5. The expression was induced by isopropyl β-D-1-thiogalactopyranoside (IPTG) (final concentration of 1 mM) and cells grew for another 24 hours under the same condition. Cells were harvested after 24 hours.

3.2 Protein purification

After disruption of the cells under pressure (FRENCH® pressure cell), affinity chromatography was used to isolate MBP from other proteins. After several times of dialysis with different buffers, MBP was separated from maltose. The denatured proteins were refolded by drop dilution and concentrated by an ion-exchange chromatography.

3.2.1 Chromatography

Chromatography is a commonly used method to separate the constituents, in order to purify a component, or to analyze a mixture. An affinity chromatography is based on a high affinity of the desirable component of the mixture to the matrix of the column (Berg et al., 2011). After elution, the desired component will be collected as a solution for further investigations. In this work, amylose bound to a column was utilized to isolate MBP from other proteins, and a buffer containing maltose (ASP2) was used to eluate MBP. Figure 18 shows a diagram of the elution of MBPwt as an example.

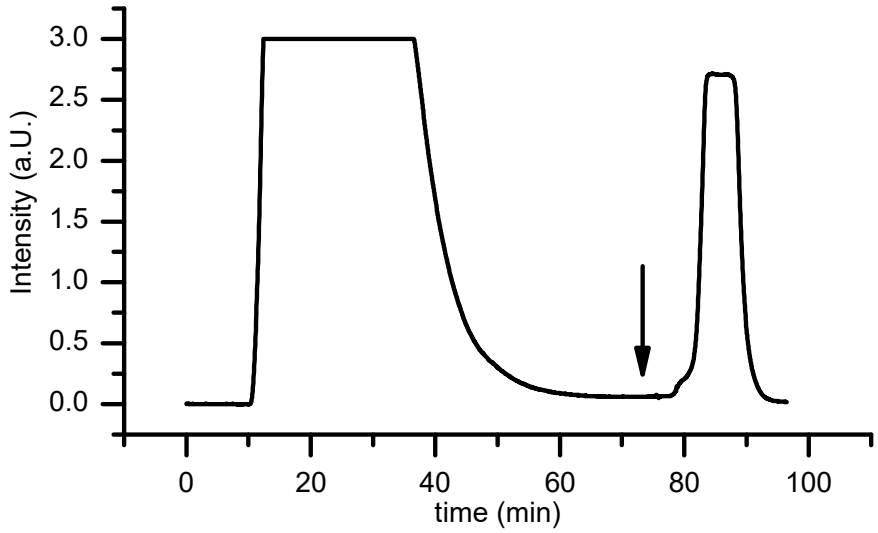

Figure 18. Diagram of affinity chromatography for isolating MBPwt

The arrow indicates the moment when the elution buffer was added. The absorbance at 280 nm indicates the presence of proteins only, due to the absorption of aromatic amino acids, which appear in almost all proteins. The first peak indicates all proteins except MBP, which was bound to the matrix of the column. Due to the limitation of the spectrophotometer, the intensity above 3 cannot be detectable, so that it was shown as 3 artificially. After the absorbance stabilized at basal level again, the elution buffer (ASP2) was applied. The eluate was collected from the moment the absorbance was above 0.1. The second peak indicated the appearance of MBPwt.

In order to remove maltose, dialysis was applied (see below). After dialysis, MBP was denatured, thus drop dilution was used to refold MBP to its native state. After that, the huge volume of MBP solution was concentrated using ion exchange chromatography (Figure 19). Ion exchange chromatography is based on electrostatic interaction. Considering the isoelectric point (pI) of MBPwt (5.22, calculated with the web tool “compute pI/Mw”, ExPASy, see reference), an anion exchanger (Q-sepharose) was used, as the buffer was adjusted to pH 8.

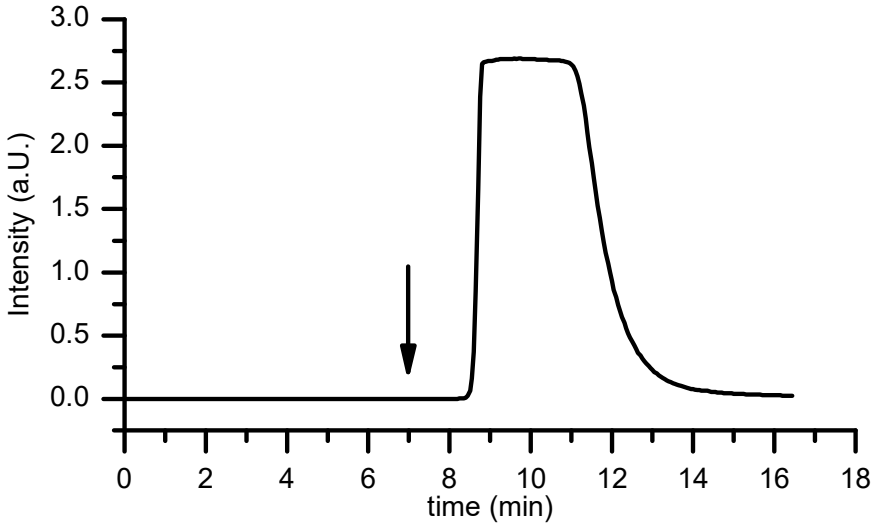

Figure 19. Diagram of ion exchange chromatography for concentrating MBPwt
The arrow indicates the moment when the elution buffer was added. Alike to the affinity chromatography, the presence of proteins was monitored at 280 nm. During sample loading MBP was bound to the anion exchanger, therefore there was no peak apparent before starting the elution. After adding the elution buffer (QSP2), which contained a high concentration of NaCl, MBP was eluted and collected.

3.2.2 Dialysis

Dialysis is an important technique to exchange buffers or to desalt a sample. It is based on a semipermeable membrane (Berg et al., 2011), which possesses a certain pore size (molecular weight cutoff MWCO). Small molecules (e.g. salt) can pass through the membrane freely, while large molecules (e.g. proteins) are held back. The driving force of distribution of the small molecules in the entire volume is the concentration gradient (Burgess, Deutscher, 2009). So the volume of the target buffer should be several times larger than for the sample, and after a certain time, a volume of fresh target buffer should replace the old one, in order to have the process continued (Figure 20). After elution of MBP from amylose-matrix, the MBP sample with bound maltose contained unbound maltose as well, due to elution buffer ASP2. In this work, the MBP

sample with bound maltose was a dialyzed with ASP1 buffer at first, to remove the unbound maltose. Next step was dialysis with QSP1-6U buffer, which contained 6 M urea. 6 M urea denatures MBP, so that the bound maltose is released and can be removed. After refolding of MBP by drop dilution, the MBP sample was concentrated by ion chromatography. After that, the sample was dialyzed with CGH5 buffer to desalt and remove Tris, which interferes with the activity of the enzymes in the maltose assay kit from Sigma Aldrich.

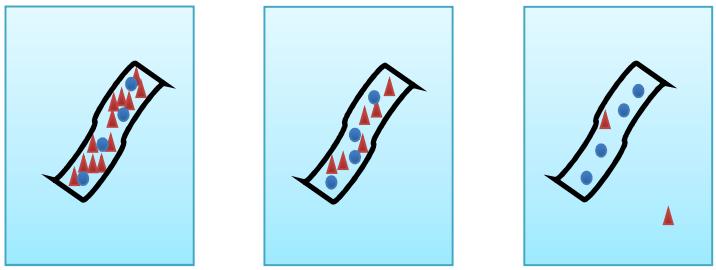

Figure 20. Schematic illustration of dialysis (Burgess, Deutscher, 2009) (modified)
The different stages of dialysis are shown: a) at the beginning, b) after renewal of buffer, and c) at the end of dialysis. Protein is shown as blue circle, salt as red triangle, the semipermeable membrane is a black pipe.

3.2.3 Drop dilution

Drop dilution achieves refolding of proteins without aggregation. High concentration of proteins during refolding can lead to aggregation; hence, the denatured protein sample will be given to the target buffer in drops under slight stirring (Burgess, Deutscher, 2009). The volume of the target buffer should be several times larger than for the sample, to avoid protein-protein interactions. In order to add the sample dropwise, a pump was used, the speed of which was set so, that the next drop fell only after the veil of the last drop had disappeared (Figure 21).

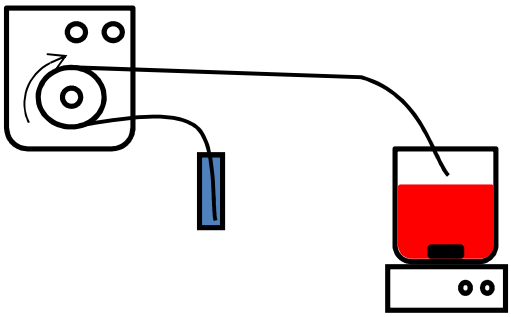

Figure 21. Schematic illustration of drop dilution
The sample is colored blue; the target buffer is red.

3.3 Characterization of MBP in both native and molten globule state

The purity of MBP was controlled by sodium dodecyl sulfate polyacrylamide gel electrophoresis (SDS-PAGE) and matrix-assisted laser desorption/ionization time-of-flight mass spectrometry (MALDI-TOF MS). The concentration was determined by different spectrophotometric methods. The molten globule state was monitored by fluorescence spectroscopy using ANS.

3.3.1 MALDI-TOF MS

MALDI is a commonly used technique for the analysis of biomolecules. A highly UV-absorbing substance is used to create a matrix, in which the biomolecules are embedded. This matrix helps biomolecules to ionize in its entirety (James, 2001), while a direct ionization method, such as electron ionization (EI), would lead to fragmentation (Hesse et al., 2005). In this work, the matrix 2,5-dihydroxybenzoic acid (DHB) was used. For instance the protein MBP is mixed with a 1000 to 10000 fold molar excess of the matrix solution and transferred to the sample target plate. Upon solvent evaporation protein and matrix molecules form crystals which are exposed to a short laser pulse. The energy of the laser pulse leads to desorption of matrix molecules and then

dissipates into the crystal lattice. A small amount of the embedded proteins is transferred as ions into the gas phase (ionization) (Meyers, 2006). The mechanism of ionization is still subject of debate. After ionization, proteins are accelerated by an electric field. The acquired kinetic energy of the ions is given by:

$$E_{kin} = \frac{1}{2}mv^2 = zeU \qquad (3.3.1\text{-}1)$$

E_{kin}: kinetic energy of ions

m: mass of ions

v: velocity of ions after the acceleration in the field

z: charge number

e: elementary charge

U: voltage of the electric field

After acceleration, the ions drift in a field-free region. The flight time and the flight length together give the velocity:

$$v = \frac{l}{t} \qquad (3.3.1\text{-}2)$$

v: velocity of ions in the field-free region

l: flight length

t: flight time

Combining the equation (3.3.1-2) and (3.3.1-1) gives

$$\frac{m}{z} = \frac{2eU}{l^2} t^2 \qquad (3.3.1\text{-}3)$$

which gives the connection between the mass to charge ratio of ions and their flight time (Meyers, 2006).

As an example the MALDI-TOF mass spectrum of MBPwt is shown in Figure 22.

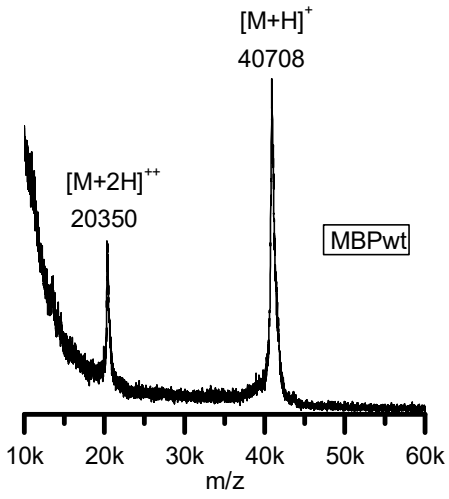

Figure 22. MALDI-TOF spectrum of MBPwt
These two peaks represent simple and double charged MBPwt ions. The result (40708 Da) matches with a calculated mass of 40707.32 Da (calculated with the web tool "compute pI/Mw", ExPASy, see reference).

3.3.2 Protein concentration determination

Determination of the concentration of protein samples is a basic technique in biochemistry. Depending on the demand for the accuracy and the required time, there are two methods used in this work.

3.3.2.1 Bicinchoninic acid (BCA) assay

The BCA assay is a rapid method to determine the concentration of proteins, similar to the Lowry protein assay. It is based on a color reaction between Cu^{+} and bicinchoninate in alkaline milieu. The protein reduces the copper(II) ion to copper(I) ion, which forms a complex with two bicinchoninate molecules. This complex can be measured at 562 nm (Richter, 2003). However, this test is a relative test, which requires a calibration curve with a standard protein solution such as bovine serum albumin (BSA). For measurements needing higher accuracy, the concentration would be determined by UV-vis spectroscopy.

3.3.2.2 UV-vis spectroscopy

UV-vis spectroscopy is a method to determine the concentration of protein (280 nm) directly, based on the Beer-Lambert law (Figure 23) (Wedler, 1997).

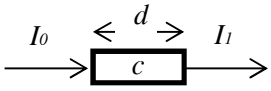

Figure 23. Schematic illustration of the process of UV-vis photometry (Wedler, 1997) (modified)
I_0 is the intensity of the light beam before entering the sample, while I_1 is intensity of the transmitted light beam after the sample; d is the length of the path inside the sample; c is the concentration of the sample.

The correlation of the absorbance and the concentration is given by

$$A = -\log\frac{I_1}{I_0} = \varepsilon \cdot c \cdot d \qquad (3.3.2.2\text{-}1)$$

A: absorbance (dimensionless)

I_1: intensity of the transmitted light

I_0: intensity of the light before entering the sample

ε: molar absorption coefficient ($mM^{-1}cm^{-1}$)

c: concentration of the sample (mM)

d: thickness of the sample (cm)

The molar absorption coefficient depends on the molecular species, for MBPwt it is 66.35 $mM^{-1}*cm^{-1}$ (calculated with the "ProtParam tool", ExPASy, see reference). The absorbance can be measured, so the concentration is

$$c = \frac{A}{\varepsilon \cdot d} \qquad (3.3.2.2\text{-}2)$$

3.3.3 Fluorescence spectroscopy

As mentioned before, the molten globule state is a partially denatured state. The considerable part of the hydrophobic side chains of proteins are exposed to the protein surface and bind to the dye ANS (Mulqueen, Kronman, 1982, Semisotnov et al., 1991). Using fluorescence spectroscopy, the molten globule state can be monitored.

For this measurement, the samples contained 1 µM protein and 100 µM ANS. CGH5 buffer was used. Excitation wavelength was 380 nm, and the emission was recorded from 400 nm to 550 nm. For each pH value a blank with proteins and a blank with ANS were measured and subtracted from the sample spectrum.

3.3.4 Verify the absence of maltose with maltose assay

After isolation of MBP from other proteins, the bound maltose was removed using dialysis. The absence of maltose was confirmed with a maltose assay, based on enzymatic reactions (Figure 24). The concentration of maltose is proportional to that of NAPDH, which has an absorption maximum at 340 nm, therefore the presence of maltose can be monitored (Bergmeyer, 1974). The Figure 24 represents the reactions schematically.

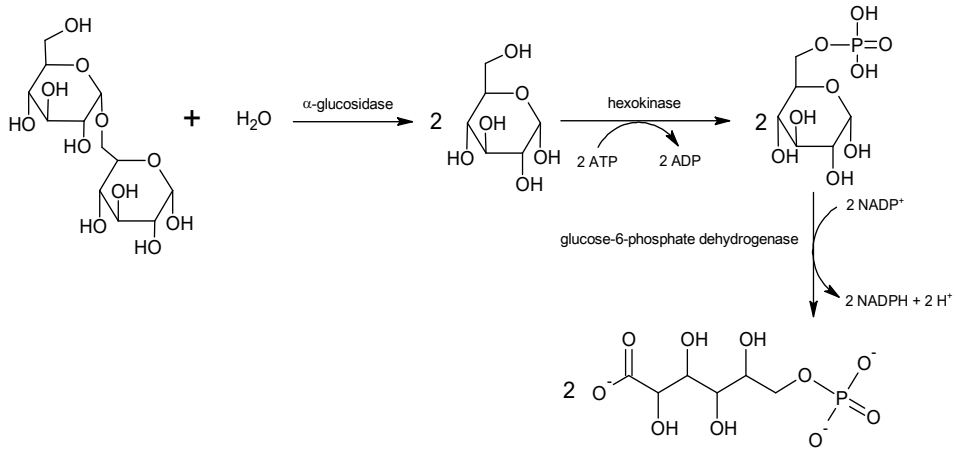

Figure 24. Schematic representation of enzymatic reactions from maltose to 6-phosphogluconate (Bergmeyer, 1974)
The cofactor $NADP^+$ was turned to NADPH, which can be measured at 340 nm. According to the Beer-Lambert law, the concentration of NADPH can be calculated, which is twice the concentration of maltose.

In order to release the bound maltose, a 0.2 mM MBP sample was heated at 98 °C for 10 minutes to denature MBP first. The procedure of this test is according to the enclosed protocol of the maltose assay kit (Sigma Aldrich). Due to an additional dye in this kit, a purple color was observed in the presence of maltose and the absorbance was measured at 570 nm. This dye could be the tetrazolium dye e.g. 3-(4,5-dimethylthiazol-2-yl)-2,5-diphenyltetrazolium bromide (MTT),

which can be reduced by NAD(P)H-dependent oxidoreductase (Mosmann, 1983, Berridge, Tan, 1993). Tris buffer interferes with the activity of the enzymes in this kit, so the sample should be dialyzed to remove Tris before.

4 RESULTS AND CONCLUSIONS

4.1 Far-UV-CD data of MBPwt in the native and molten globule state fitted by NLSF

In a previous work, MBPwt in the molten globule state was investigated with far-UV-CD spectroscopy (Chakour, 2015). At that time, we could just recognize the difference between the native and the molten globule state, also the difference between the presence and the absence of maltose at pH 3. In the meantime, we can analyze the spectra quantitatively with NLSF according to the protocol of Kemmer and Keller (Kemmer, Keller, 2010). The spectra of secondary structures in the paper of Brahms (Brahms, Brahms, 1980) were used as reference spectra. In Figure 25 the far-UV-CD spectra and the corresponding fit curves are demonstrated.

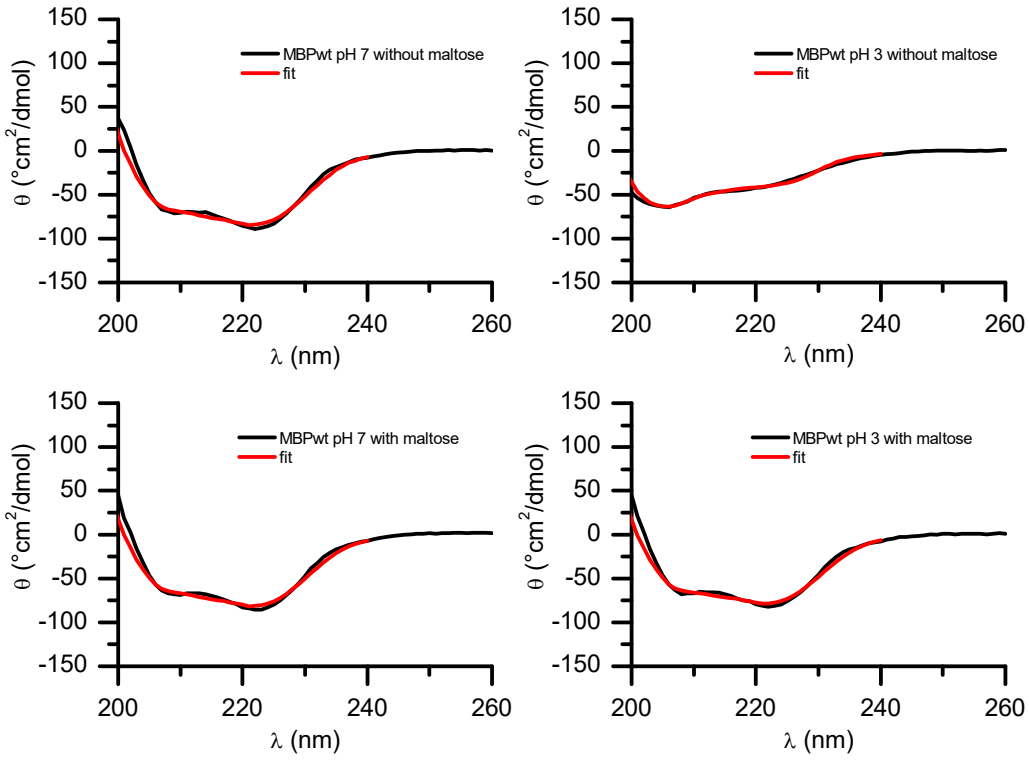

Figure 25. The far-UV-CD spectra and the corresponding fit curves of MBPwt with and without maltose at pH 7 and pH 3

The fit curves coincide with the spectra well, and the extracted proportion of the defined secondary structures is listed in Table 2.

Table 2. The fitted proportion of the listed secondary structure features

	Without maltose		With maltose	
	pH 7	pH 3	pH 3	pH 7
$f_{\alpha\text{-helix}}$	38% (33%, 43%)	25% (21%, 34%)	38% (33%, 58%)	38% (32%, 43%)
$f_{\beta\text{-sheet}}$	21% (0, 28%)	25% (11%, 38%)	21% (0, 45%)	21% (0, 46%)
$f_{\beta\text{-turn}}$	14% (3%, 27%)	2% (0, 11%)	14% (2% 19%)	14% (2%, 20%)
$f_{\text{random coil}}$	27% (0, 59%)	48% (35%, 62%)	27% (0, 59%)	27% (0, 61%)

The confidence interval with confidence level of 95% is given in parathesis. It is calculated with Fisher's F distribution (Kemmer, Keller, 2010).

The proportions of four defined secondary structural features and the corresponding confidence intervals are almost identical in the presence of maltose at both pH values. In the absence of maltose, the relation of these features and the confidence intervals at pH 7 are still comparable with those in the presence of maltose. These imply a native-like secondary structure in the molten globule state in the presence of maltose. In the absence of maltose at pH 3, the proportions of the listed features are totally changed as compared to the presence of maltose: the percentage portion of β-turn decreases by 86%, whereas that of random coil increases by 78%; α-helix is degraded visibly (by 34%), while of β-sheet is a little more constructed (by 19%). This suggests that MBP loses even some secondary structure in the molten globule state without maltose. It gives also a clue that the presence of maltose affects the buildup of secondary structure, even the folding of MBP.

4.2 Maltose assay

The presence of maltose can result in conformational changes; furthermore, it can affect the binding affinity measured by the ITC experiment. Therefore, a maltose assay should be performed to confirm the absence of maltose in samples of MBP.

This test requires a calibration curve for calculating the concentration of maltose in samples of proteins. However, a qualitative characterization suffices for our purpose. Figure 26 and Table 3 to Table 5 show the results of the maltose assay.

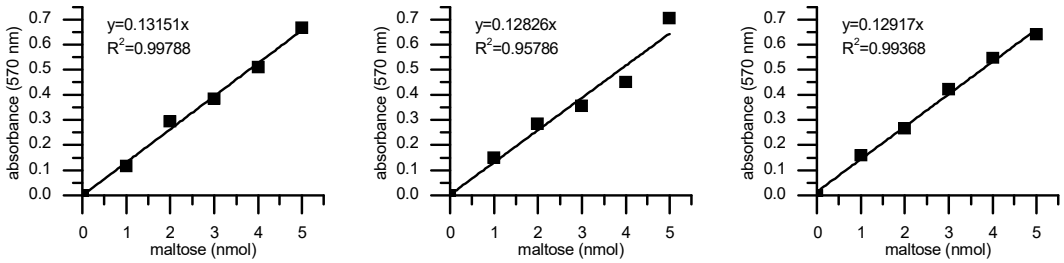

Figure 26. Calibration curves with the standard samples of the maltose assay kit

Due to the presence of maltose in some samples (e.g. MBP1, highlighted in yellow, see Table 3), the measurements were repeated with corresponding calibrations. The three calibrations were used for determination of samples MBPwt, MBP2, 4, 7, and 8 (left), for MBP1, 3 and 6 (middle) and for MBP5 and MBP12 (right), respectively.

Table 3. The measured absorbance values of the samples MBPwt, MBP1, 2, 4, 7 and 8, and the calculated concentration of maltose in the samples

Substance	Concentration of the substance (mM)	Absorbance	Absorbance minus blank	Calculated concentration of maltose (mM)
Blank	0	0.057	0.000	-
MBPwt	0.2	0.043	-0.014	<LOQ
MBP1	0.2	0.221	0.164	0.1
MBP2	0.2	0.052	-0.005	<LOQ
MBP4	0.2	0.058	0.001	<LOQ
MBP7	0.2	0.056	-0.001	<LOQ
MBP8	0.2	0.053	-0.004	<LOQ
Maltose (p.c.)	0.2	0.663	0.606	0.2

p.c.: positive control; LOQ: 0.04 mM

Table 4. The measured absorbance values of the samples MBP1, 3 and 6, and the calculated concentration of maltose in the samples

Substance	Concentration of the substance (mM)	Absorbance	Absorbance minus blank	Calculated concentration of maltose (mM)
Blank	0	0.044	0.000	-
MBP1	0.2	0.047	0.003	<LOQ
MBP3	0.2	0.045	0.001	<LOQ
MBP6	0.2	0.044	0.000	<LOQ
Maltose (p.c.)	0.2	0.514	0.470	0.2
Buffer (n.c.)	0	0.048	0.004	<LOQ

p.c.: positive control; n.c.: negative control; LOQ: 0.04 mM

Table 5. The measured absorbance values of the samples MBP5 and MBP12, and the calculated concentration of maltose in samples

Substance	Concentration of the substance (mM)	Absorbance	Absorbance minus blank	Calculated concentration of maltose (mM)
Blank	0	0.048	0.000	-
MBP5	0.2	0.049	0.001	<LOQ
MBP12	0.2	0.050	0.002	<LOQ
Maltose (p.c.)	0.2	0.628	0.580	0.2
Buffer (n.c.)	0	0.045	-0.003	<LOQ

p.c.: positive control; n.c.: negative control; LOQ: 0.04 mM

It is explicit that maltose in all of the samples of MBP was unobservable. If there were observable maltose, the sample would be dialyzed with QSP1-6U again and this test repeated.

4.3 Fluorescence spectroscopy with ANS

The molten globule state can be stabilized at low pH (Dolgikh et al., 1981). In order to verify this pH value for MBP, fluorescence spectroscopy with ANS was performed. The excitation wavelength was 380 nm (Sheshadri et al., 1999), while the emission was recorded from 400 nm to 550 nm. The spectra show that the emission maximum emerged at 472 nm, thus the emission at 472 nm against pH values has been shown in Figure 27.

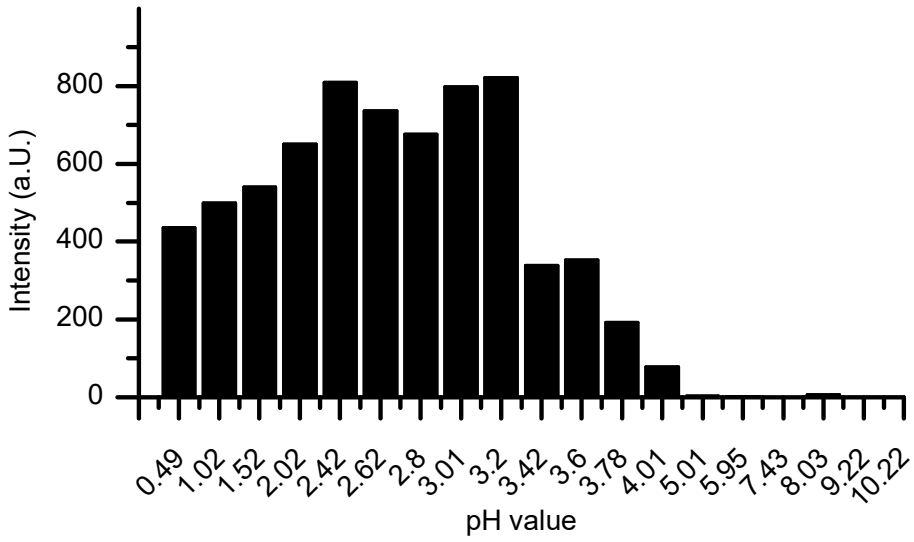

Figure 27. Fluorescence spectroscopy of MBPwt using ANS

It is clear that there is a maximum of the intensity of fluorescence at pH 3.20 (821), which indicates a (partially) denatured structure. This agrees with the finding of Sheshadri *et al* (Sheshadri et al., 1999).

The far-UV-CD spectra suggest that the presence of maltose affects the formation of secondary structures. In order to verify the effect of maltose to the formation of molten globule state of MBP, the fluorescence spectroscopy with the samples, which contained maltose additionally, was performed. The excitation wavelength was 380 nm, while the emission was recorded from 400 nm to 550 nm. Again a maximum emission at 472 nm was observed and shown in Figure 28 as function of pH.

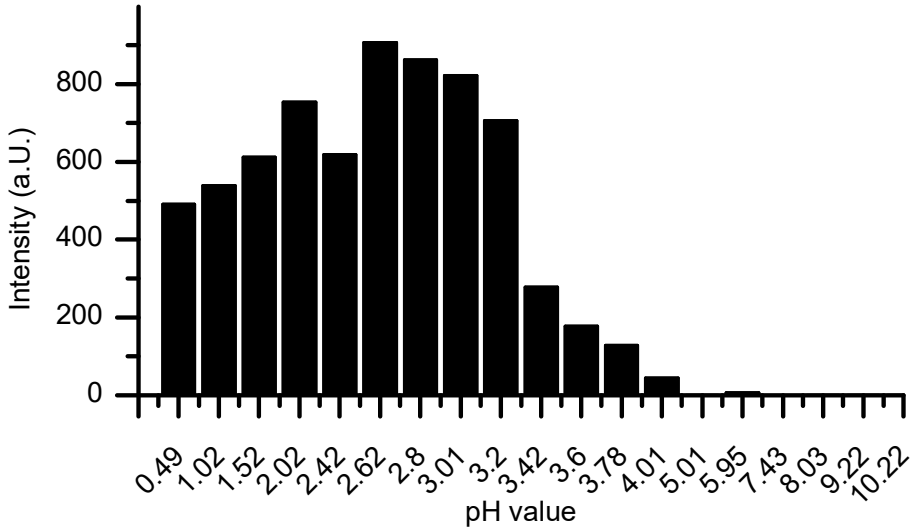

Figure 28. Fluorescence spectroscopy of MBPwt with maltose using ANS

The intensity at pH 3.20 (706) is smaller than that under unliganded condition. This indicates that the exposed hydrophobic side chains are reburied through the binding to maltose. The maximum of the intensity shifts to pH 2.62 (906), which indicates the maximal exposure of hydrophobic side chains in the presence of maltose. Is it still a molten globule state? How does it affect protein folding? To answer these questions a further investigation is needed, which is beyond the scope of this work.

4.4 MBP1 to MBP7 investigated by pulsed EPR

The double mutants MBP1 to MBP7 in the molten globule state without maltose were investigated in previous work (Chakour, 2015). In this work, the effect of the ligand, maltose, on the folding of MBP was examined. The DEER experiment was performed at 50 K. The time domain signal and the corresponding distance distribution of the spin label pair of MBP5 with

maltose at pH 3 are illustrated in Figure 29. The data of MBP5 without maltose are illustrated for comparison.

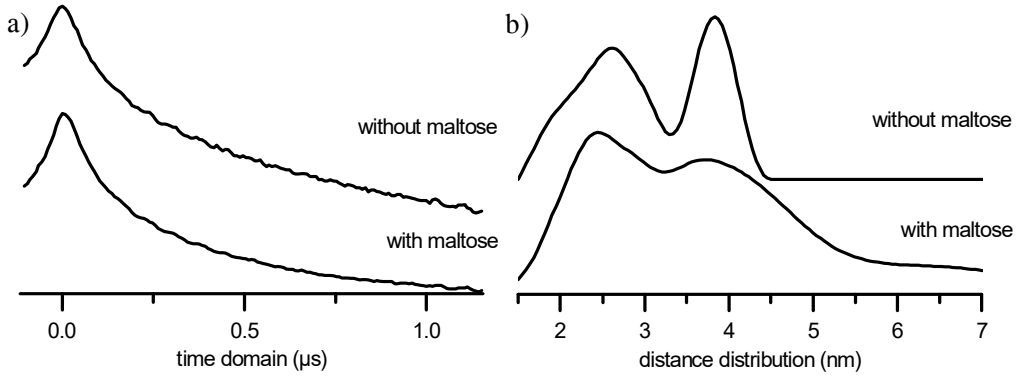

Figure 29. a) DEER time domain signals of MBP5; b) the reconstructed distance distribution
The time domain signals of DEER experiment were analyzed with DeerAnalysis using Tikhonov regularization (Jeschke et al., 2006).

The dominant interspin distances of MBP5 at pH 3 without maltose are 2.6 nm and 3.8 nm. The more probable distance is 3.8 nm. Compared to the distance distribution of MBP5 at pH 7, it is considerably broadened and exhibits several possibilities of distances, which implies the lack of tertiary structure. With maltose the distance distribution at pH 3 is still broadened, however, the short distance (2.4 nm) is more likely. This implies that, on one hand, MBP binds to maltose in its molten globule state; on the other hand, maltose stabilizes the tertiary structure at least partially in the molten globule state. Due to the collaboration with ACERT, the other double mutants were investigated by DQC experiments. What is interesting is that the dominant distance of MBP4 with maltose (4.2 nm) is larger than that without maltose (3.0 nm) (Figure 30).

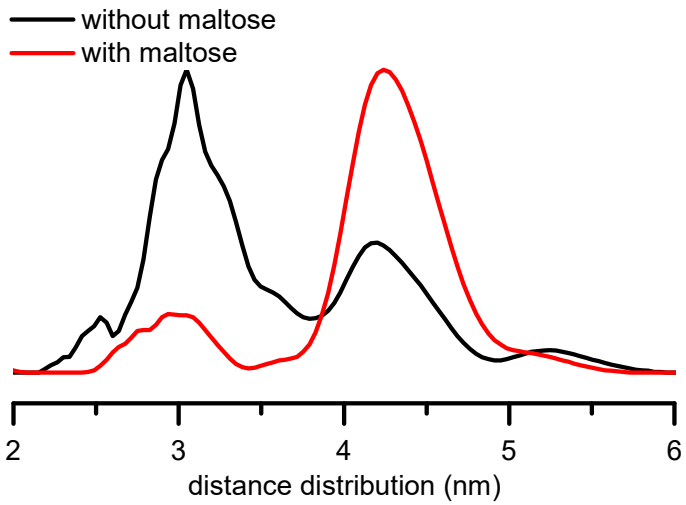

Figure 30. Reconstructed distance distribution of MBP4 at pH 3
The DQC data were analyzed with the maximum-entropy method (Chiang et al., 2005).

In order to understand this distance change, we took a look at the crystal structure (Figure 31).

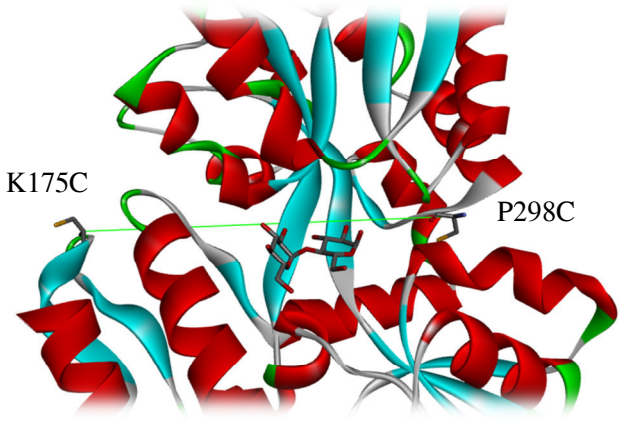

Figure 31. Representation of MBP4 with Discovery Studio Visualizer BIOVIA (PBD ID: 1anf, modified)
The mutated cysteines are displayed as stick structure with associated names P298C and K175C. In the middle of the picture, the maltose molecule is shown as stick structure. The perspective is from the top of the binding pocket down to the bottom.

The interspin distance of MBP4 is the distance between a β-sheet (K175C) and a random coil (P298C), which links a α-helix and a β-sheet. In the molten globule state, without maltose, this distance is smaller than that with maltose. It is reasonable to visualize that the bottom of MBP is bending, because of the binding to maltose, so that the top of the two domains get closer to each other. This confirms the findings of Quiocho *et al* (Quiocho et al., 1997).

Based on these findings, the further investigations with other double mutants in the presence of maltose at both pH values were required. The distance distributions of the double mutants MBP1, 2, 3, 6 and 7 determined by DQC experiment are illustrated in Figure 32.

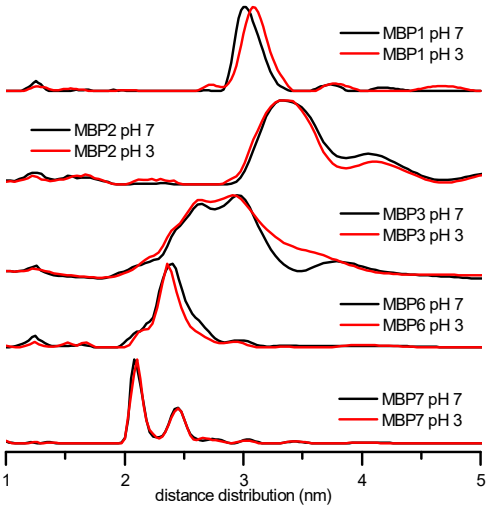

Figure 32. The reconstructed distance distribution of MBP1, 2, 3, 6 and 7 with maltose

The results show clearly that the distance distributions of each double mutant are comparable at both pH values. This coincides with the assumption from the far-UV-CD results and the DEER data of MBP5, which is maltose stabilizes (partially) the tertiary structures.

In order to confirm the binding of MBP to maltose at pH 3, ITC measurements were performed.

4.5 ITC measurement

The binding affinity of MBP was determined by an ITC measurement. For comparison, MBPwt at pH 7 was measured as well. The parameters are listed in the appendix. The Figure 33 demonstrates the titration diagrams and the associated fit diagrams of MBPwt at pH 7 and pH 3.

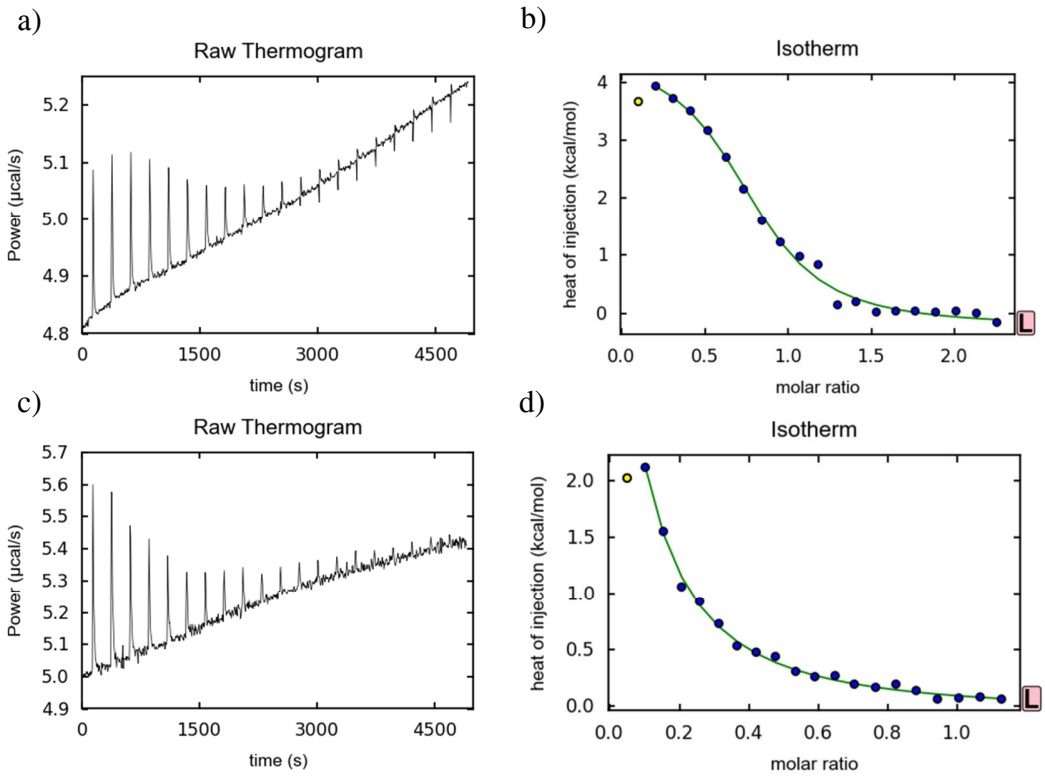

Figure 33. ITC experiments with MBPwt titrated with maltose at 5 °C

Figure a) shows the diagram of differential heating power against time at pH 7.5; and b) is the diagram of integrated heat (blue circle) against molar ratio with NITPIC at pH 7.5. Figure c) shows the diagram of differential heating power against time at pH 3.2; and d) is integrated heat (blue circle) against molar ratio with NITPIC at pH 3.2. The first injections, which are not considered during further data analysis, are shown as yellow circle. Green lines are fit curves with NITPIC (Keller et al., 2012). The heat of buffer dilution is small compared to the heat of binding. The binding site is obtained as nearly one.

Because of the long equilibration time and the possible error of preparation of the syringe before measurement, the first injection is generally considered as outlier.

The measurement at each pH value was performed in triplicate. In order to analyze the results at each pH value globally, SEDPHAT is used (Figure 34).

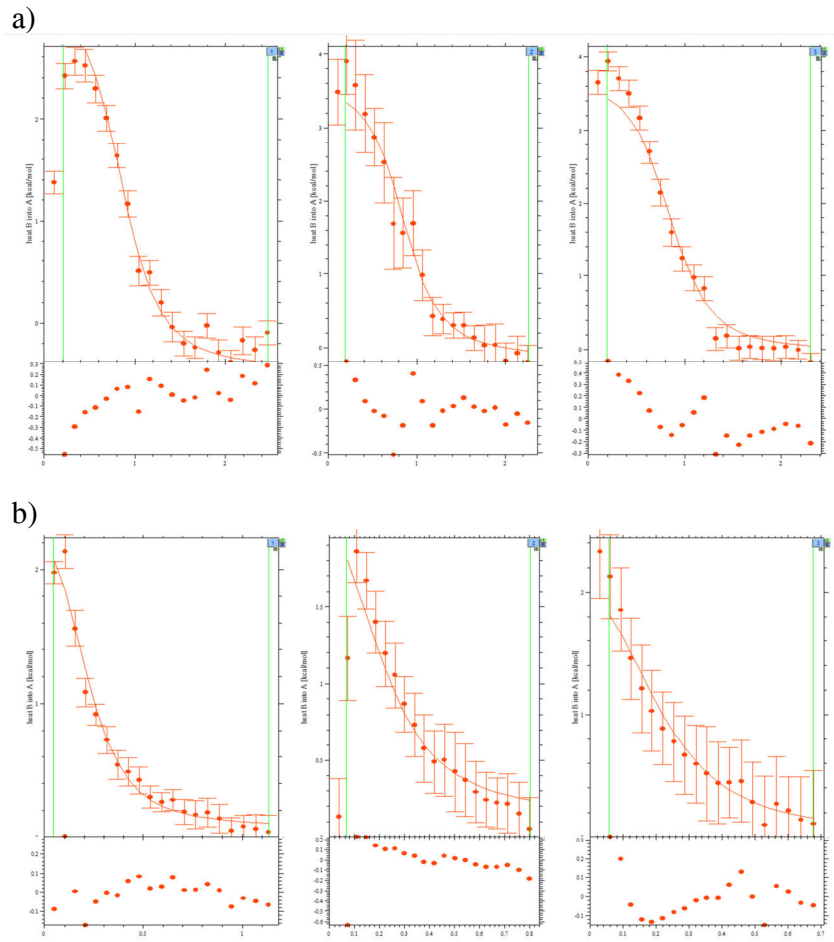

Figure 34. Global fit curves of ITC data with SEDPHAT

Figure a) is integrated heat against molar ratio with error bars at pH 7.5 (5 °C); and b) is integrated heat against molar ratio with error bars at pH 3.2 (5 °C). The points between the green lines are fitted (Schuck, 2000). At pH 3.2, the first measurement was carried out with different concentrations of MBP and maltose as for the second and third measurements. In spite of this, the results arising from the measurement at pH 3.2 are capable for global fit.

The integrated heat decreases progressively at both pH values with the increasing molar ratio of maltose to MBP. The fit curves indicate an endothermal reaction.

The fitted thermodynamic parameters and the calculated Gibbs free energy ΔG and entropy change ΔS, together with the literature values, are listed in Table 6. The confidence intervals of ΔH are calculated with Fisher's F distribution with a confidence level of 95%, whereas the confidence interval of K_d are calculated from the intervals of lgK_a.

Table 6. Thermodynamic parameters of binding of MBPwt to maltose

MBPwt	K_d (μM)	ΔH (kcal/mol)	ΔG (kcal/mol)	$-T\Delta S$ (kcal/mol)
pH 7.5 (5 °C)	2.6 (1.0, 6.3)	3.8 (3.2, 4.7)	-7.1 (-7.6, -6.6)	-10.9 (-11.3, -10.8)
Lit (pH 7.0, 25 °C)[#]	1.3±0.6*	2.3±0.1	-7.9±0.2	-10.2±0.1
pH 3.2 (5 °C)	28.8 (12.6, 66.1)	2.6 (2.1, 3.7)	-5.8 (-6.2, -5.3)	-8.4 (-9.0, -8.3)
Lit (pH 3.0, 25 °C)[#]	33.3±0.8*	1.6±0.1	-6.0±0.3	-7.5±0.2

*: Converted values from the given literature with calculated errors by propagation of uncertainty (Bevington, 1969).

[#]: value from Prajapati *et al* (Prajapati et al., 2007).

In spite of the different measuring temperatures, the measured values in this work are comparable with the literature values. The binding affinity at pH 3.2 is 11 fold lower than for pH 7.5. Gibbs free energy ΔG at pH 7.5 is lower than at pH 3.2, which coincides with the fact that binding of MBP to maltose is more stable in the native state than for the molten globule state. The term associated with entropy change $-T\Delta S$ is larger at pH 3.2 than at pH 7.5, while the enthalpy change ΔH is smaller at pH 3.2 than at pH 7.5. These findings indicate that binding of MBP to maltose in the molten globule state goes from more disordered to ordered structures than in the native state on one side, on the other side binding beginning with more disordered

structures is more favorable than with ordered structure. This coincides with the finding from the far-UV-CD spectroscopy.

4.6 Mutagenesis of the new double mutant MBP12

It is confirmed that MBP binds maltose at pH 3. The next interesting question is whether the tertiary structure of the binding pocket is built without maltose in the molten globule state, or maltose induces the formation of the tertiary structure of the binding pocket. To answer this question, we need to investigate such double mutants, of which the cysteine pairs are distributed near the binding pocket. MBP8 (P298C S233C) was previously generated by my colleague Benjamin Selmke, of which the mutated cysteine pair distributes near the binding pocket. In my work, an independent double mutant MBP12 (G13C T237C) was designed to indicate the distance variation near the binding pocket of MBP. In order to obtain the template of the wild type, the MBP6 was used for mutagenesis. Then the wild type was mutated to MBP12. The associated DNA sequences are listed in the appendix. In Figure 35 only part of this sequence with the mutated bases is shown.

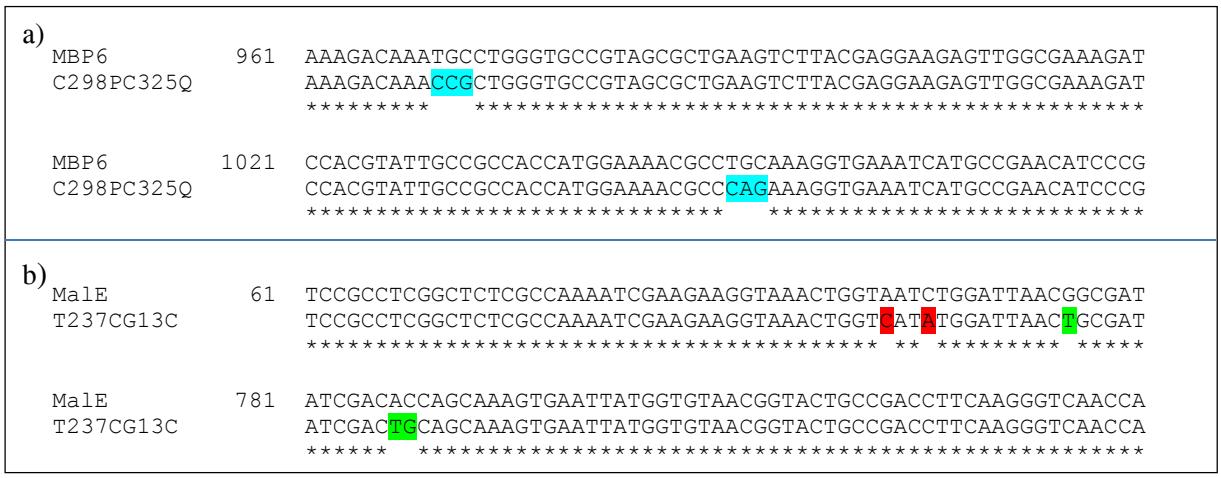

Figure 35. Part of the aligned DNA sequences of the a) MBP6 vs MBPwt and b) MBPwt vs MBP12
The bases, which are mutated from MBP6 back to the wild type, are colored cyan. The bases, which are mutated from MBPwt to MBP12 in order to be translated to cysteines, are colored green. Red color marks the silent mutation, which introduces a new cutting site for NdeI.

According to the codon table, the cysteine of MBP6 coded by TGC was mutated to proline coded by CCG; and the other cysteine, also coded by TGC, was mutated to glutamine coded by CAG. After the double mutagenesis, the translated amino acid sequence coincides with that of MBPwt, which indicates the successful mutagenesis.

The same work was performed for mutagenesis of MBP12. The successful mutations of glycine (GGC) to cysteine (TGC) and of threonine (ACC) to cysteine (TGC) are colored green. The further mutations of GTA to GTC and of ATC to ATA do not change the amino acid valine and isoleucine, respectively, but introduce a new cutting site for restriction enzyme NdeI (5' CA|TATG 3'). The mutation of threonine to cysteine introduces by itself a new cutting site for PstI (5' CTGCA|G 3'), fortunately. The introduced new cutting sites facilitate the

identification of the successful mutating by digestion with the corresponding restriction enzymes. The MBP12 and MBP8 are illustrated in the crystal structure in Figure 36.

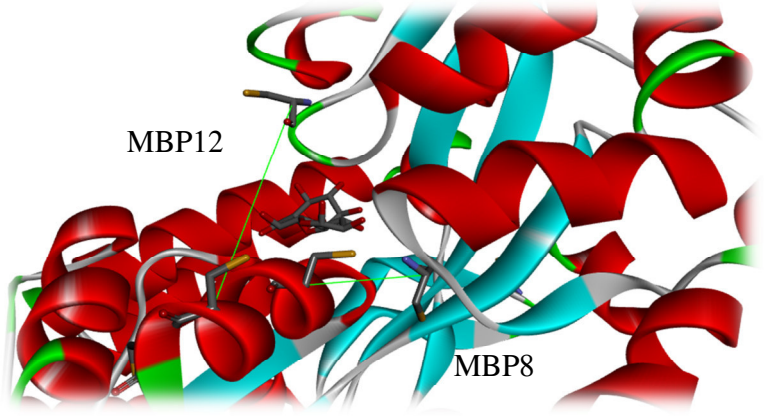

Figure 36. Representation of MBP12 and MBP8 with Discovery Studio Visualizer BIOVIA (PBD ID: 1anf, modified)
The mutated cysteines are displayed as stick structure. The cysteine pairs are connected by green lines and indicated with associated mutant names. In the middle of the picture, the maltose molecule is shown as stick structure. The perspective is from one side with two domains distributed in top right and bottom left.

4.7 MBP8 and MBP12 investigated by CW EPR

The new double mutants MBP8 and MBP12 were investigated by CW EPR at pH 3.2 and pH 7.4. The spectra are summarized in Figure 37. At each pH value the double mutant was measured with and without maltose.

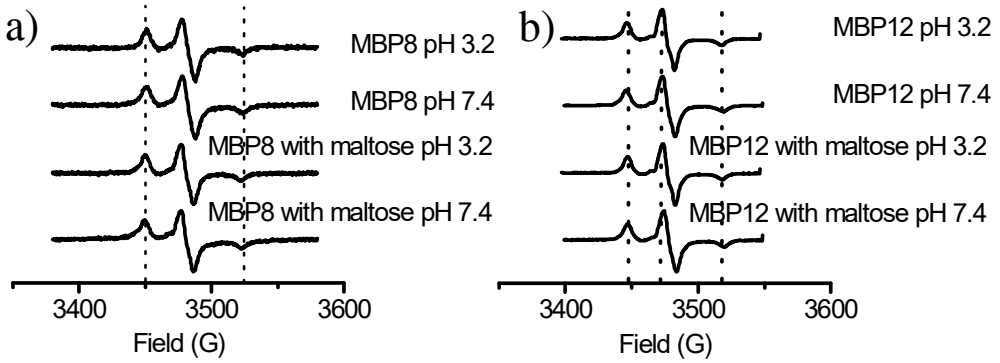

Figure 37. CW spectra of a) MBP8 and b) MBP12 at 150 K

It appears that there is hardly any difference between the four spectra of each double mutant. For direct comparison, the mean distance and the distribution width fitted by DIPFIT (Steinhoff et al., 1997) are listed in Table 7.

Table 7. The mean interspin distance and the distribution width of MBP8 and MBP12

		Without maltose		With maltose	
		pH 3.2	pH 7.4	pH 3.2	pH 7.4
MBP8	Mean distance (nm)	1.3	1.1	1.2	0.8
	Width (nm)	1.1	0.8	0.9	0.3
MBP12	Mean distance (nm)	1.5	1.7	1.6	1.6
	Width (nm)	0.4	0.3	0.4	0.4

At pH 3.2 the interspin distances of MBP8 are similar, regardless of the presence of maltose, and so are the distribution widths of MBP8. At pH 7.4 the mean distance and distribution width of MBP8 without maltose is still comparable with those at pH 3.2. However, MBP8 with maltose at

pH 7.4 shows a deviation of mean distance and distribution width compared to those under other conditions. This can be due to the fluctuation of the tertiary structure in the molten globule state. On the contrary, MBP12 shows nearly no variation of distances and distribution widths in both pH values, even in the absence of maltose.

4.8 Conclusion

The fitting of the far-UV-CD spectra gives us a clue to understand the effect of ligand binding on protein folding. MBP in the molten globule state preserves a large part of α-helix and β-sheet; however, it loses also some secondary structure, so that more random coil structures appear. Through binding to maltose, one of the ligands of MBP, the secondary structure is considerably regained, as to be comparable with that in the native state. In the native state, ligand binding has no effect on the secondary structure of MBP, which implies this binding process concerns primarily the tertiary structures.

The fluorescence spectroscopy with ANS indicates the pH value, at which MBP folds in the molten globule state (Semisotnov et al., 1991). As expected, the maximal intensity of fluorescence lies on pH 3.2 (Sheshadri et al., 1999). ANS is a dye, which specifically binds to nonpolar molecules (Stryer, 1965). This means ANS binds to the hydrophobic side chains of MBP at pH 3.2, which is due to the loss of tertiary structures and additionally some secondary structure details (see above). After addition of maltose, the intensity of fluorescence decreases at pH 3.2, which indicates the exposed hydrophobic side chains are reburied. This coincides with the results of far-UV-CD spectroscopy.

The peripheral structures of MBP are investigated by double mutants MBP1 to MBP7. With the assumption arising from far-UV-CD spectroscopy and fluorescence spectroscopy, it is interesting

to find out the interspin distance variation of double mutants arising from EPR. MBP shows an indeterminate tertiary structure between the different regions of MBP which leads to the broadened distance distributions and the increased possibilities of alternative distances of MBP1 to MBP7 (Chakour, 2015). In the presence of maltose, the distance distributions differ from that without maltose, which implies that MBP binds to maltose in the molten globule state. The binding process of MBP to maltose in the molten globule state has been confirmed by ITC experiment, in spite of 11 fold lower affinity than in the native state. This process (at 5 °C) is more favorable with entropy change in the native state than in the molten globule state, due to the undetermined tertiary structure and the exposure of the hydrophobic side chains in the molten globule state, which leads to an increase of disorder. However, this process is more favorable with enthalpy change in the molten globule state than in the native state, which indicates binding with disordered structures is more facile than with ordered structures. These findings show a greater structural change during binding in the molten globule state than in the native state, which coincides with the findings arising from far-UV-CD spectroscopy and fluorescence spectroscopy. Vamvaca *et al*. obtained similar results with the chorismate mutase from *Methanococcus jannaschii*. Their interpretation is that the molten globule of chorismate mutase undergoes structural ordering during ligand binding and the tightening of the molten globule supports the global packing interactions (Vamvaca et al., 2008).

The little difference between the interspin distance distribution in the molten globule state and the native state in the presence of maltose indicates that the tertiary structure of MBP is reasonably rebuilt. It means that maltose stabilizes at least partially the tertiary structure of MBP. These findings coincide with the conclusion of Vamvaca *et al*, which is, the ligand can stabilize the protein and furthermore lead to an improvement of global packing (Vamvaca et al., 2004).

Is it a ligand-induced conformational change in the binding pocket (Koshland, 1958)? Or is the binding pocket a highly ordered region in the molten globule? To answer the questions, we need to focus on the surrounding of the binding pocket investigated by the double mutants MBP8 and MBP12. There are nearly no differences of the mean distance and distribution width at both pH values arising from the CW spectra of MBP12. Furthermore, maltose does not result in a change of mean distances of MBP12 in the native and the molten globule state. These results suggest a definite structure near the binding pocket of MBP. This confirms the assumption of Prajapati *et al*. (Prajapati et al., 2007). Although MBP 8 shows a broadened width at pH 3.2, the mean distances are still comparable, except under the condition pH 7.4 with maltose. It can be that DIPFIT can only give an average distance, and the change of the distances arising from the DIPFIT-analysis of CW spectra of MBP8 at different pH values could have been appeared in the form of a broadened distance width, so that it is not very sensitive to analyze distance distributions. Hence, the further investigation of MBP8 by DQC experiments is required.

In summary, MBP contains a highly ordered tertiary structure around the binding pocket in the molten globule state, which leads to the binding of maltose. In turn, maltose stabilizes the rest of the structure to re-form more tertiary structure details. These findings help us to better understand the mechanism of protein folding, which is relevant for developing a model of protein folding and furthermore for a strategy of drug design, as well as for the treatment of diseases. In the future, double mutants with cysteine pairs on a site of the binding pocket different from those in MBP8 and MBP12 can be prepared. Together with the investigation of MBP8 and MBP12 with more methodologies, they can give more details about the structural changes during ligand binding in the molten globule state.

5 REFERENCES

Banham, J. E.; Baker, C. M.; Ceola, S.; Day, I. J.; Grant, G. H.; Groenen, E. J. J.; Rodgers, C. T.; Jeschke, G.; Timmel, C. R. Distance measurements in the borderline region of applicability of CW EPR and DEER: a model study on a homologous series of spin-labelled peptides. *Journal of magnetic resonance (San Diego, Calif. : 1997)* **2008,** *191* (2), 202–218.

Berg, J. M.; Tymoczko, J. L.; Stryer, L.; Häcker, B. *Biochemie*, Korr. Nachdr. der 6. Aufl.; Spektrum Akad. Verl.: Heidelberg, **2011**.

Bergmeyer, H. U., Ed., 3. neubearb. und erw. Aufl.; *Methoden der enzymatischen Analyse;* Verl. Chemie: Weinheim/Bergstr., **1974**.

Berliner, L. J. *Spin Labeling*. *Theory and Applications;* Elsevier Science: Burlington, **1976**.

Berliner, L. J. *Spin labeling*. *Theory and applications;* Ed.; Biological magnetic resonance 8; Plenum Pr: New York, **1989**.

Berliner, L. J. *Distance measurements in biological systems by EPR;* Ed.; Biological magnetic resonance 19; Kluwer: New York, NY, **2000**.

Berridge, M. V.; Tan, A. S. Characterization of the cellular reduction of 3-(4,5-dimethylthiazol-2-yl)-2,5-diphenyltetrazolium bromide (MTT): subcellular localization, substrate dependence, and involvement of mitochondrial electron transport in MTT reduction. *Archives of Biochemistry and Biophysics* **1993**, 303 (2), 474–482.

Bevington, P. R. *Data reduction and error analysis for the physical sciences;* McGraw-Hill: New York [etc.], **1969**.

Borbat, P. P.; Freed, J. H. Multiple-quantum ESR and distance measurements. *Chemical Physics Letters* **1999,** *313* (1-2), 145–154.

Borbat, P. P.; Freed, J. H. Pulse Dipolar Electron Spin Resonance: Distance Measurements. In *Structural Information from Spin-Labels and Intrinsic Paramagnetic Centres in the Biosciences*; Timmel, C. R., Harmer, J. R., Eds.; Structure and Bonding; Springer Berlin Heidelberg: Berlin, Heidelberg, **2013**; pp 1–82.

Brahms, S.; Brahms, J. Determination of protein secondary structure in solution by vacuum ultraviolet circular dichroism. *Journal of Molecular Biology* **1980,** *138* (2), 149–178.

Burgess, R. R.; Deutscher, M. P. *Guide to protein purification*, 2nd ed.; Methods in enzymology v. 463; Elsevier/Academic Press: Amsterdam, Boston, **2009**.

Chakour, M. Strukturuntersuchungen verschiedener Mutanten des Maltose-Bindungsproteins (MBP) mit Hilfe der ESR Spektroskopie, Dissertation, TU Kaiserslautern, **2015**.

Chiang, Y.-W.; Borbat, P. P.; Freed, J. H. Maximum entropy: A complement to Tikhonov regularization for determination of pair distance distributions by pulsed ESR. *Journal of Magnetic Resonance* **2005,** *177* (2), 184–196.

Dolgikh, D. A.; Gilmanshin, R. I.; Brazhnikov, E. V.; Bychkova, V. E.; Semisotnov, G. V.; Venyaminov, S.; Ptitsyn, O. B. α-lactalbumin: Compact state with fluctuating tertiary structure? *FEBS Letters* **1981,** *136* (2), 311–315.

Ganesh, C.; Shah, A. N.; Swaminathan, C. P.; Surolia, A.; Varadarajan, R. Thermodynamic characterization of the reversible, two-state unfolding of maltose binding protein, a large two-domain protein. *Biochemistry* **1997,** *36* (16), 5020–5028.

Hahn, E. L. Spin Echoes. *Phys. Rev.* **1950,** *80* (4), 580–594.

Hellmann, N.; Jaenicke, E.; Decker, H. Two types of urate binding sites on hemocyanin from the crayfish Astacus leptodactylus: An ITC study. *Biophysical Chemistry* **2001,** *90* (3), 279–299.

Hesse, M.; Meier, H.; Zeeh, B. *Spektroskopische Methoden in der organischen Chemie*. *102 Tabellen*, 7., überarb. Aufl.; Thieme electronic book library; Thieme: Stuttgart, **2005**.

Hubbell, W. L.; Altenbach, C. Investigation of structure and dynamics in membrane proteins using site-directed spin labeling. *Current opinion in structural biology* **1994,** *4* (4), 566–573.

James, P. *Proteome research: mass spectrometry;* Ed.; Principles and practice; Springer: Berlin, **2001**.

Jeschke, G. Distance Measurements in the Nanometer Range by Pulse EPR. *ChemPhysChem* **2002,** *3* (11), 927–932.

Jeschke, G. DEER distance measurements on proteins. *Annual review of physical chemistry* **2012,** *63*, 419–446.

Jeschke, G.; Chechik, V.; Ionita, P.; Godt, A.; Zimmermann, H.; Banham, J.; Timmel, C. R.; Hilger, D.; Jung, H. DeerAnalysis2006—a comprehensive software package for analyzing pulsed ELDOR data. *Appl. Magn. Reson.* **2006,** *30* (3-4), 473–498.

Johnson, M. L. Why, when, and how biochemists should use least squares. *Analytical Biochemistry* **1992,** *206* (2), 215–225.

Junk, M. J. N. *Assessing the Functional Structure of Molecular Transporters by EPR Spectroscopy;* Springer Berlin Heidelberg: Berlin, Heidelberg, **2012**.

Kataoka, M.; Kuwajima, K.; Tokunaga, F.; Goto, Y. Structural characterization of the molten globule of alpha-lactalbumin by solution X-ray scattering. *Protein science : a publication of the Protein Society* **1997,** *6* (2), 422–430.

Keller, S.; Vargas, C.; Zhao, H.; Piszczek, G.; Brautigam, C. A.; Schuck, P. High-precision isothermal titration calorimetry with automated peak-shape analysis. *Analytical chemistry* **2012,** *84* (11), 5066–5073.

Kemmer, G.; Keller, S. Nonlinear least-squares data fitting in Excel spreadsheets. *Nature protocols* **2010,** *5* (2), 267–281.

Koshland, D. E. Application of a Theory of Enzyme Specificity to Protein Synthesis. *Proceedings of the National Academy of Sciences* **1958,** *44* (2), 98–104.

Leavitt, S.; Freire, E. Direct measurement of protein binding energetics by isothermal titration calorimetry. *Current opinion in structural biology* **2001,** *11* (5), 560–566.

Levinthal, C. *How to fold graciously*. In Mossbauer Spectroscopy in Biological Systems: Proceedings of a meeting held at Allerton House, Monticello, Illinois (**1969**), pp. 22-24.

Meyers, R. A. *Encyclopedia of Analytical Chemistry;* Ed.; John Wiley & Sons, Ltd: Chichester, UK, **2006**.

Mosmann, T. Rapid colorimetric assay for cellular growth and survival: Application to proliferation and cytotoxicity assays. *Journal of Immunological Methods* **1983**, 65 (1-2), 55–63.

Mulqueen, P. M.; Kronman, M. J. Binding of naphthalene dyes to the N and A conformers of bovine α-lactalbumin. *Archives of Biochemistry and Biophysics* **1982,** *215* (1), 28–39.

Oldham, M. L.; Chen, S.; Chen, J. Structural basis for substrate specificity in the Escherichia coli maltose transport system. *Proceedings of the National Academy of Sciences of the United States of America* **2013,** *110* (45), 18132–18137.

Pannier, M.; Veit, S.; Godt, A.; Jeschke, G.; Spiess, H. W. Dead-time free measurement of dipole–dipole interactions between electron spins. *Journal of Magnetic Resonance* **2011,** *213* (2), 316–325.

Prajapati, R. S.; Indu, S.; Varadarajan, R. Identification and thermodynamic characterization of molten globule states of periplasmic binding proteins. *Biochemistry* **2007,** *46* (36), 10339–10352.

Quiocho, F. A.; Spurlino, J. C.; Rodseth, L. E. Extensive features of tight oligosaccharide binding revealed in high-resolution structures of the maltodextrin transport/chemosensory receptor. *Structure* **1997,** *5* (8), 997–1015.

Rabenstein, M. D.; Shin, Y. K. Determination of the distance between two spin labels attached to a macromolecule. *Proceedings of the National Academy of Sciences of the United States of America* **1995,** *92* (18), 8239–8243.

Richter, G. *Praktische Biochemie*. *Grundlagen und Techniken ; 19 Tabellen;* Thieme: Stuttgart, **2003**.

Roessler, M. M.; King, M. S.; Robinson, A. J.; Armstrong, F. A.; Harmer, J.; Hirst, J. Direct assignment of EPR spectra to structurally defined iron-sulfur clusters in complex I by double electron-electron resonance. *Proceedings of the National Academy of Sciences of the United States of America* **2010,** *107* (5), 1930–1935.

Schuck, P. Size-Distribution Analysis of Macromolecules by Sedimentation Velocity Ultracentrifugation and Lamm Equation Modeling. *Biophysical journal* **2000,** *78* (3), 1606–1619.

Schwarzinger, S.; Mohana-Borges, R.; Kroon, G. J.; Dyson, H. J.; Wright, P. E. Structural characterization of partially folded intermediates of apomyoglobin H64F. *Protein science : a publication of the Protein Society* **2008,** *17* (2), 313–321.

Semisotnov, G. V.; Rodionova, N. A.; Razgulyaev, O. I.; Uversky, V. N.; Gripas', A. F.; Gilmanshin, R. I. Study of the "molten globule" intermediate state in protein folding by a hydrophobic fluorescent probe. *Biopolymers* **1991,** *31* (1), 119–128.

Sheshadri, S.; Lingaraju, G. M.; Varadarajan, R. Denaturant mediated unfolding of both native and molten globule states of maltose binding protein are accompanied by large deltaCp's. *Protein science : a publication of the Protein Society* **1999,** *8* (8), 1689–1695.

Spurlino, J. C.; Lu, G. Y.; Quiocho, F. A. The 2.3-A resolution structure of the maltose- or maltodextrin-binding protein, a primary receptor of bacterial active transport and chemotaxis. *The Journal of biological chemistry* **1991,** *266* (8), 5202–5219.

Steinhoff, H. J.; Radzwill, N.; Thevis, W.; Lenz, V.; Brandenburg, D.; Antson, A.; Dodson, G.; Wollmer, A. Determination of interspin distances between spin labels attached to insulin: comparison of electron paramagnetic resonance data with the X-ray structure. *Biophysical journal* **1997,** *73* (6), 3287–3298.

Stryer, L. The interaction of a naphthalene dye with apomyoglobin and apohemoglobin. *Journal of Molecular Biology* **1965,** *13* (2), 482–495.

Vamvaca, K.; Jelesarov, I.; Hilvert, D. Kinetics and thermodynamics of ligand binding to a molten globular enzyme and its native counterpart. *Journal of Molecular Biology* **2008,** *382* (4), 971–977.

Vamvaca, K.; Vogeli, B.; Kast, P.; Pervushin, K.; Hilvert, D. An enzymatic molten globule: efficient coupling of folding and catalysis. *Proceedings of the National Academy of Sciences of the United States of America* **2004,** *101* (35), 12860–12864.

Wang, W.; Malcolm, B. A. Two-stage PCR protocol allowing introduction of multiple mutations, deletions and insertions using QuikChange Site-Directed Mutagenesis. *BioTechniques* **1999,** *26* (4), 680–682.

Wedler, G. *Lehrbuch der physikalischen Chemie*, 4., völlig überarb. und erw. Aufl.; Wiley-VCH: Weinheim, **1997**.

Weil, J. A.; Bolton, J. R.; Wertz, J. E. *Electron paramagnetic resonance. Elementary theory and practical applications*; A Wiley Interscience publication; Wiley: New York, **1994**.

Wertz, J. E.; Bolton, J. R. *Electron spin resonance. Elementary theory and pract. applications*, Reprint d. Ausg. New York **1972**; Chapman and Hall: New York, **1986**.

Wolynes, P.; Onuchic, J.; Thirumalai, D. Navigating the folding routes. *Science* **1995,** *267* (5204), 1619–1620.

Zheng, L.; Baumann, U.; Reymond, J.-L. An efficient one-step site-directed and site-saturation mutagenesis protocol. *Nucleic acids research* **2004,** *32* (14), e115.

6 APPENDIX

Materials and equipment

Plasmid

The *MalE* gene was cloned into the vector pMalp2, which has also been used as a template for the mutagenesis of the double mutants MBP1 to MBP7. The double mutants were designed with one mutated cysteine in the binding pocket and the other mutated cysteine located on one of the two domains of the MBP. With the same template, the plasmids of the double mutants MBP8 and MBP12 were mutated in a manner, that each pair of cysteines was located near the binding pocket. The information about the position of the double mutants is listed in Table A 1.

Table A 1. Position of the mutated cysteines of each double mutant

	1st mutation	2nd mutation
MBP1	P298C	T31C
MBP2	P298C	D82C
MBP3	P298C	N124C
MBP4	P298C	K175C
MBP5	P298C	K313C
MBP6	P298C	Q325C
MBP7	P298C	S238C
MBP8	P298C	S233C
MBP12	G13C	T237C

The results of sequencing are listed below, the signal sequence is colored red.

>MBP6
ATGAAAATAAAAACAGGTGCACGCATCCTCGCATTATCCGCATTAACGACGATGATGTTTTCCGCCTCGGCTCTCGC
CAAAATCGAAGAAGGTAAACTGGTAATCTGGATTAACGGCGATAAAGGCTATAACGGTCTCGCTGAAGTCGGTAAGA
AATTCGAGAAAGATACCGGAATTAAAGTCACCGTTGAGCATCCGGATAAACTGGAAGAGAAATTCCCACAGGTTGCG
GCAACTGGCGATGGCCCTGACATTATCTTCTGGGCACACGACCGCTTTGGTGGCTACGCTCAATCTGGCCTGTTGGC
TGAAATCACCCCGGACAAAGCGTTCCAGGACAAGCTGTATCCGTTTACCTGGGATGCCGTACGTTACAACGGCAAGC
TGATTGCTTACCCGATCGCTGTTGAAGCGTTATCGCTGATTTATAACAAAGATCTGCTGCCGAACCCGCCAAAAACC
TGGGAAGAGATCCCGGCGCTGGATAAAGAACTGAAAGCGAAAGGTAAGAGCGCGCTGATGTTCAACCTGCAAGAACC
GTACTTCACCTGGCCGCTGATTGCTGCTGACGGGGGTTATGCGTTCAAGTATGAAAACGGCAAGTACGACATTAAAG
ACGTGGGCGTGGATAACGCTGGCGCGAAAGCGGGTCTGACCTTCCTGGTTGACCTGATTAAAAACAAACACATGAAT
GCAGACACCGATTACTCCATCGCAGAAGCTGCCTTTAATAAAGGCGAAACAGCGATGACCATCAACGGCCCGTGGGC
ATGGTCCAACATCGACACCAGCAAAGTGAATTATGGTGTAACGGTACTGCCGACCTTCAAGGGTCAACCATCCAAAC
CGTTCGTTGGCGTGCTGAGCGCAGGTATTAACGCCGCCAGTCCGAACAAAGAGCTGGCGAAAGAGTTCCTCGAAAAC
TATCTGCTGACTGATGAAGGTCTGGAAGCGGTTAATAAAGACAAATGCCTGGGTGCCGTAGCGCTGAAGTCTTACGA
GGAAGAGTTGGCGAAAGATCCACGTATTGCCGCCACCATGGAAAACGCCTGCAAAGGTGAAATCATGCCGAACATCC
CGCAGATGTCCGCTTTCTGGTATGCCGTGCGTACTGCGGTGATCAACGCCGCCAGCGGTCGTCAGACTGTCGATGAA
GCCCTGAAAGACGCGCAGACTCGTATCACCAAGTAA

>pMALp2MalE
ATGAAAATAAAAACAGGTGCACGCATCCTCGCATTATCCGCATTAACGACGATGATGTTTTCCGCCTCGGCTCTCGC
CAAAATCGAAGAAGGTAAACTGGTAATCTGGATTAACGGCGATAAAGGCTATAACGGTCTCGCTGAAGTCGGTAAGA
AATTCGAGAAAGATACCGGAATTAAAGTCACCGTTGAGCATCCGGATAAACTGGAAGAGAAATTCCCACAGGTTGCG
GCAACTGGCGATGGCCCTGACATTATCTTCTGGGCACACGACCGCTTTGGTGGCTACGCTCAATCTGGCCTGTTGGC
TGAAATCACCCCGGACAAAGCGTTCCAGGACAAGCTGTATCCGTTTACCTGGGATGCCGTACGTTACAACGGCAAGC
TGATTGCTTACCCGATCGCTGTTGAAGCGTTATCGCTGATTTATAACAAAGATCTGCTGCCGAACCCGCCAAAAACC
TGGGAAGAGATCCCGGCGCTGGATAAAGAACTGAAAGCGAAAGGTAAGAGCGCGCTGATGTTCAACCTGCAAGAACC
GTACTTCACCTGGCCGCTGATTGCTGCTGACGGGGGTTATGCGTTCAAGTATGAAAACGGCAAGTACGACATTAAAG
ACGTGGGCGTGGATAACGCTGGCGCGAAAGCGGGTCTGACCTTCCTGGTTGACCTGATTAAAAACAAACACATGAAT
GCAGACACCGATTACTCCATCGCAGAAGCTGCCTTTAATAAAGGCGAAACAGCGATGACCATCAACGGCCCGTGGGC
ATGGTCCAACATCGACACCAGCAAAGTGAATTATGGTGTAACGGTACTGCCGACCTTCAAGGGTCAACCATCCAAAC
CGTTCGTTGGCGTGCTGAGCGCAGGTATTAACGCCGCCAGTCCGAACAAAGAGCTGGCGAAAGAGTTCCTCGAAAAC
TATCTGCTGACTGATGAAGGTCTGGAAGCGGTTAATAAAGACAAACCGCTGGGTGCCGTAGCGCTGAAGTCTTACGA
GGAAGAGTTGGCGAAAGATCCACGTATTGCCGCCACCATGGAAAACGCCCAGAAAGGTGAAATCATGCCGAACATCC
CGCAGATGTCCGCTTTCTGGTATGCCGTGCGTACTGCGGTGATCAACGCCGCCAGCGGTCGTCAGACTGTCGATGAA
GCCCTGAAAGACGCGCAGACTCGTATCACCAAGTAA

>MBP12
ATGAAAATAAAAACAGGTGCACGCATCCTCGCATTATCCGCATTAACGACGATGATGTTTTCCGCCTCGGCTCTCGC
CAAAATCGAAGAAGGTAAACTGGTCATATGGATTAACTGCGATAAAGGCTATAACGGTCTCGCTGAAGTCGGTAAGA
AATTCGAGAAAGATACCGGAATTAAAGTCACCGTTGAGCATCCGGATAAACTGGAAGAGAAATTCCCACAGGTTGCG
GCAACTGGCGATGGCCCTGACATTATCTTCTGGGCACACGACCGCTTTGGTGGCTACGCTCAATCTGGCCTGTTGGC
TGAAATCACCCCGGACAAAGCGTTCCAGGACAAGCTGTATCCGTTTACCTGGGATGCCGTACGTTACAACGGCAAGC
TGATTGCTTACCCGATCGCTGTTGAAGCGTTATCGCTGATTTATAACAAAGATCTGCTGCCGAACCCGCCAAAAACC
TGGGAAGAGATCCCGGCGCTGGATAAAGAACTGAAAGCGAAAGGTAAGAGCGCGCTGATGTTCAACCTGCAAGAACC
GTACTTCACCTGGCCGCTGATTGCTGCTGACGGGGGTTATGCGTTCAAGTATGAAAACGGCAAGTACGACATTAAAG
ACGTGGGCGTGGATAACGCTGGCGCGAAAGCGGGTCTGACCTTCCTGGTTGACCTGATTAAAAACAAACACATGAAT
GCAGACACCGATTACTCCATCGCAGAAGCTGCCTTTAATAAAGGCGAAACAGCGATGACCATCAACGGCCCGTGGGC
ATGGTCCAACATCGACTGCAGCAAAGTGAATTATGGTGTAACGGTACTGCCGACCTTCAAGGGTCAACCATCCAAAC
CGTTCGTTGGCGTGCTGAGCGCAGGTATTAACGCCGCCAGTCCGAACAAAGAGCTGGCGAAAGAGTTCCTCGAAAAC
TATCTGCTGACTGATGAAGGTCTGGAAGCGGTTAATAAAGACAAACCGCTGGGTGCCGTAGCGCTGAAGTCTTACGA
GGAAGAGTTGGCGAAAGATCCACGTATTGCCGCCACCATGGAAAACGCCCAGAAAGGTGAAATCATGCCGAACATCC
CGCAGATGTCCGCTTTCTGGTATGCCGTGCGTACTGCGGTGATCAACGCCGCCAGCGGTCGTCAGACTGTCGATGAA
GCCCTGAAAGACGCGCAGACTCGTATCACCAAGTAA

Genotype of the competent *E. coli*

NEB5α competent E. coli

fhuA2 Δ(argF-lacZ)U169 phoA glnV44 Φ80 Δ(lacZ)M15 gyrA96 recA1 relA1 endA1 thi-1 hsdR17

BL21(DE3) competent E. coli

fhuA2 [lon] ompT gal (λ DE3) [dcm] ΔhsdS

λ DE3 = λ sBamHIo ΔEcoRI-B int::(lacI::PlacUV5::T7 gene1) i21 Δnin5

Buffers for cell culture

Lysogeny Broth medium (500 ml)

12.5 g LB medium

500 ml H_2O_{dd}

autoclave

store at 4 °C

Terrific Broth medium (500 ml)

25.4 g TB medium

500 ml H_2O_{dd}

add 2 ml glycerol before autoclave

autoclave

store at 4 °C

LB-Amp-Agar Petri dish (20 pieces)

12.5 g LB medium

7.5 g agar-agar

500 ml H_2O_{dd}

autoclave and cool down to 40 °C

add 500 µl ampicillin stock solution

divide into 20 portions

store at 4 °C

Ampicillin stock solution (10 ml)

1 g ampicillin-sodium salt

add autoclaved H_2O_{dd} to 10 ml

vortex and apply sterile filtration

store at -20 °C

IPTG stock solution (5 ml)

1.192 g IPTG

add autoclaved H_2O_{dd} to 5 ml

vortex and apply sterile filtration

store at -20 °C

Buffers for protein purification

ASP1 buffer (1 L)

2.42 g Tris

11.69 g NaCl

900 ml H_2O_{dd}

adjust pH value to 7.4

add H_2O_{dd} to 1 L

sterile filtration

store at 4 °C

ASP2 buffer (1 L)

2.43 g Tris

1.46 g NaCl

3.60 g maltose monohydrate

900 ml H_2O_{dd}

adjust pH value to 7.4

add H_2O_{dd} to 1 L

sterile filtration

store at 4 °C

QSP1 buffer (5 L)

12.12 g Tris

5.85 g NaCl

add H_2O_{dd} to 5 L

adjust pH value to 8

sterile filtration

store at 4 °C

QSP2 buffer (1 L)

2.43 g Tris

58.44 g NaCl

900 ml H_2O_{dd}

adjust pH value to 8

add H_2O_{dd} to 1 L

sterile filtration

store at room temperature

QSPR buffer (500 ml)

2.43 g Tris

116.88 g NaCl

900 ml H_2O_{dd}

adjust pH value to 8

add H_2O_{dd} to 1 L

sterile filtration

store at room temperature

QSP1-6U buffer (5 L)

12.12 g Tris

5.85 g NaCl

1803.75 g urea

add H_2O_{dd} to 5 L

adjust pH value to 8

store at room temperature

CGH5 buffer (1 L)

1.47 g sodium citrate

0.38 g glycine

1.19 g HEPES

add H_2O_{dd} to 1 L

adjust pH value as needed

store at 4 °C

SDS stock solution (1 L)

1 g SDS

add H_2O_{dd} to 1 L

sterile filtration

store at room temperature

Ethanol stock solution (1 L)

200 ml ethanol

800 ml H_2O_{dd}

store at room temperature

Buffers for spin labeling

DTT stock solution (10 ml)

0.15 g DTT

add H_2O_{dd} to 10 ml

vortex and apply sterile filtration

store at 4 °C

MTS stock solution (1 ml)

26.45 mg MTS

1 ml dry acetonitrile

dissolve under nitrogen

store at -80 °C

Buffers for SDS-PAGE

1.875 M Tris-HCl (100 ml)

22.7 g Tris

add H_2O_{dd} to 100 ml

adjust pH value to 8.8 with HCl

store at 4 °C

0.6 M Tris-HCl (100 ml)

7.2 g Tris

add H_2O_{dd} to 100 ml

adjust pH value to 6.8 with HCl

store at 4 °C

APS solution (10% w/v) (10 ml)

1 g APS

add H_2O_{dd} to 10 ml

SDS solution (10% w/v) (50 ml)

5 g SDS

50 ml H_2O_{dd}

SDS sample buffer (4x) (10 ml)

5 ml Tris-HCl (1 M, pH 6.8)

4 ml glycerol (87%)

1 g SDS

0.16 g bromophenol blue

add H_2O_{dd} to 10 ml

immediately before use add DTT (62 mg/10 ml)

Electrophoresis stock solution (10x) (2 L)

288 g glycine

60 g Tris

20 g SDS

add H_2O_{dd} to 2 L

adjust pH value to 8.3 with HCl

Electrophoresis solution (1x) (1 L)

100 ml electrophoresis stock solution

900 ml H_2O_{dd}

Table A 2. Pipetting protocol of SDS-gel

	Resolving gel (12%)	Stacking gel (5%)
30% acylamide	3.64 ml	655 µl
1.875 M Tris-HCl (pH 8.8)	1.9 ml	-
0.6 M Tris-HCl (pH 6.8)	-	393 µl
H_2O_{dd}	3.36 ml	2.84 ml
SDS (10%)	89.7 µl	39.3 µl
TEMED	10 µl	5 µl
APS (10%)	75 µl	25 µl

Solution for BCA test

BSA solution (800 µl, 0.25 mg/ml)

100 µl BSA standard (stock solution, see below)

700 µl H_2O_{dd}

Chemicals

Agar-agar, Kobe I	Carl Roth
α-Glucosidase from *Saccharomyces cerevisiae*	recombinant, expressed in proprietary host, lyophilized powder, ≥100 units/mg protein
	Sigma-Aldrich
Ampicillin sodium salt	Carl Roth
Amylose resin	New England Biolabs
APS (ammonium persulfate)	Sigma-Aldrich
Bromophenol blue (for SDS-buffer)	Fluka
BSA standard	for protein assay 2 mg/ml BSA with 0.05% NaN3
	Interchim
D(+)-Maltose monohydrate	≥95%, für die Biochemie
	Carl Roth
DpnI	New England Biolabs
DTT (Dithiothreitol)	high purity for molecular biology
	GERBU
Ethanol	abs. reag. Ph. Eur. ≥99.8% (GC)
	Sigma-Aldrich

G6P-DH from *Saccharomyces cerevisiae*	Type XV, lyophilized powder, 200-400 units/mg protein (modified Warburg-Christian)
	Sigma-Aldrich
Glycerol	ROTIPURAN®≥99.5%, p.a., wasserfrei
	Carl Roth
Glycine	molecular biology grade
	AppliChem
HCl (hydrochloric acid)	35-38%, p.a.,
	TH.GEYER
HEPES	buffer grade
	AppliChem
Hexokinase from *Saccharomyces cerevisiae*	Type F-300, lyophilized powder, ≥130 units/mg protein (biuret)
	Sigma-Aldrich
IPTG	≥99%, für die Biochemie
	Carl Roth
Isopentane	AppliChem
Isopropanol	molecular biology grade
	AppliChem
LB-Medium (Luria/Miller)	für die Molekularbiologie
	Carl Roth
NaCl	≥99.5%, p.a., ACS, ISO
	Carl Roth
Papain aus *Carica Papaya*	Sigma-Aldrich
Phusion HF DNA polymerase	New England Biolabs
Rotiphores®Gel 30	Carl Roth
SDS (sodium dodecyl sulfate)	ultra pure, ICN Biomedicals

sodium citrate dihydrate	≥99%, p.a., ACS
	Carl Roth
TEMED	AppliChem
Terrific-Broth-Medium	für die Molekularbiologie
	Carl Roth
Tris	ultrapure
	AppliChem
Urea	EMPROVE®exp
	Merck

Disposable materials

Centrifuge tubes	Bottle PC 26.3 ml	Beckman Coulter
Concentrators	Vivaspin 6 und 20 ml, 10,000 MWCO	Sartorius
	Macrosep®Advance Centrifugal Devices10K, Pall life scienes	VWR
Dialysis tubes	Visking 1780. 1ff	Carl Roth
	Zellu Trans 12/25mm	Carl Roth
Pasteur pipette	glass, 230 mm	Roth
Pipette tips	different volume	Sarstedt, Nümbrecht
Reaction vessels	1.5 ml	Sarstedt, Nümbrecht
Sterile filters	0.2µm	Sarstedt, Nümbrecht
Tubes	15 ml, 50 ml, PP	Sarstedt, Nümbrecht

Equipment

Autoclave	Systec V-65
Centrifuges	Beckman® J2-21
	Eppendorf, Centrifuge 5415C
	Eppendorf, 5810R
Centrifuges	Stuart Rotator SB3
Drying cabinet	Heraeus
EPR	Bruker X-Band Elexsys E580 pulse spectrometer
	Dielectric Bruker Flexline resonator ER 4118X MD5 for CW EPR
	Split-ring Bruker Flexline resonator ER 4118x MS3 for pulsed EPR
Fluorescence photometer	Perkin-Elmer LS 50B
Freezers	Sanyo MDF-U3086S, Ultra Low
	Sanyo MDF-U72V, VIP™ Series, Ultra Low
FRENCH® pressure cell	SLM Instruments, INC.
Incubator	Memmert
ITC200	GE Healthcare
Laminar flow cabinet	Heraeus Instruments, Laminair® HB 2448
Magnetic stirrer	Janke und Kunkel IKA motor KMO2 electronic
MALDI	Bruker ultraflex TOF/TOF
Mini electrophoresis systems	Bio-Rad, mini-PROTEAN® Tetra cell
Minishaker	Retsch mixer
pH meter	Mettler Toledo, Inlab® micro
Pipettes	Eppendorf Research plus
	Brand Transferpette® S

Pipettes	Brand, Accu-jet® Pro
Power-supply	PowerPac 3000, Bio-Rad
Pump	Pharmacia Biotech pump P-1
Quarzcapillary	Ø3 Self-construction
Quarzcuvettes	110-QS 1 mm with certificate Hellma® Analytics
	110-QS 10 mm with certificate Hellma® Analytics
Refrigerator	Liebherr
Shakers	New Brunswick Scientific, Innova 4000, Nürtinger
	HT Infors AG, Bottmingen
Shakers	Desaga, Diffusions-Entfärbe-Apparatur, Heidelberg
Thermo shaker	Eppendorf, Thermomixer comfort
	Thermo Scientific, MaxQ 400
Ultra-Sound cell disrupter	Branson Sonic, Sonifier® B-12
UV-vis spectrometer	Eppendorf, Biophotometerplus
	Jasco V-630
	Thermoscientific Genesys 10 uv scanning
Weighing scale	Sartorius Typ 1413
	Sartorius analytic
	Mettler Toledo, Xs205 DualRange Analytical Balance

Software

DeerAnalysis2011	ETH Zurich
FL win-Lab	PerkinElmer Ltd
flexControl-ultraflex TOF/TOF	Bruker Daltonik GmbH
NITPIC 0.7.6 beta	University of Texas Southwestern Medical Center

DIPFIT	Heinz-Jürgen Steinhoff at University Osnabrück
SEDPHAT1055 beta	Peter Schuck at National Institutes of Health

Kits

BCA protein assay reagent A and B	Uptima
InstantBlueTM	Expedeon
Maltose Assay Kit	Sigma-Aldrich
NucleoSpinR Gel and PCR Clean-up	Macherey-Nagel
NucleoSpinR Plasmid (NoLid)	Macherey-Nagel
Protein-Marker III (6.6-200)	AppliChem

Web tools

compute pI/Mw	ExPASy	http://web.expasy.org/compute_pi/
ProtParam tool	ExPASy	http://web.expasy.org/protparam/

Parameters for experiments

Table A 3. Parameters for ITC measurement at pH 7.5

Experimental parameters		Injection parameters	
Total injections	20	Volume (µl)	2
Cell temperature (°C)	5	Duration (s)	4
Reference power (µcal/s)	5	Spacing (s)	240
Initial delay (s)	120	Filter period (s)	5
Syringe concentration (mM) (pH)	0.5 (pH 7.5)		

Cell concentration (mM) (pH)	0.05 (pH 7.5)		
Stirring speed (rpm)	1000		
Feedback mode/gain	High		

Table A 4. Parameters for ITC measurement at pH 3.2

Experimental parameters		Injection parameters	
Total injections	20	Volume (µl)	2
Cell temperature (°C)	5	Duration (s)	4
Reference power (µcal/s)	5	Spacing (s)	240
Initial delay (s)	120	Filter period (s)	5
Syringe concentration (mM) (pH)	2.5/1.17* (pH 3.2)		
Cell concentration (mM) (pH)	0.5/0.39* (pH 3.2)		
Stirring speed (rpm)	1000		
Feedback mode/gain	High		

*: For the first measurement, the concentration of maltose was 2.5 mM, whereas the concentration of MBPwt was 0.5 mM; for the second and the third measurements, the concentration of maltose was 1.17 mM, whereas the concentration of MBPwt was 0.39 mM.

Table A 5. Parameters for DEER measurement (MBP5)

Parameter	MBP5 (pH 3, u)	MBP5 (pH 3, l)	MBP5 (pH 7, u)	MBP5 (pH 7, l)
ν_{obs} (GHz)	9.301	9.303	9.201	9.209
Video bandwidth (MHz)	50	50	50	50
Video gain (dB)	10	10	9	7
ν_{ELDOR} (GHz)	9.220	9.230	9.129	9.143
Pulse length $(\pi/2)_{obs}$ (ns)	16	16	16	16
Pulse length $(\pi)_{obs}$ (ns)	32	32	32	32
Pulse length $(\pi)_{ELDOR}$ (ns)	24	24	20	20
ELDOR delay t (ns)	100	100	100	100
$\tau 1$ (ns)	200	200	200	200

τ2 (ns)	1200	1200	1200	1200
Acquisition trigger d_0 (ns)	372	380	380	388
Integrator gate pg (ns)	144	124	112	108
dx_{ELDOR} (ns)	8	8	8	8
No. of points	159	159	159	160

u: without maltose; l: with maltose

Table A 6. Parameters for DEER measurement (MBP7)

Parameter	MBP7 (pH 3, u)	MBP7 (pH 3, l)	MBP7 (pH 7, u)	MBP7 (pH 7, l)
ν_{obs} (GHz)	9.217	9.260	9.442	9.291
Video bandwidth (MHz)	50	50	50	50
Video gain (dB)	10	10	14	11
ν_{ELDOR} (GHz)	9.145	9.197	9.372	9.223
Pulse length $(\pi/2)_{obs}$ (ns)	16	16	16	16
Pulse length $(\pi)_{obs}$ (ns)	32	32	32	32
Pulse length $(\pi)_{ELDOR}$ (ns)	20	48	20	20
ELDOR delay t (ns)	100	100	100	100
τ1 (ns)	200	200	200	200
τ2 (ns)	1200	1200	1200	1200
Acquisition trigger d_0 (ns)	360	364	372	350
Integrator gate pg (ns)	100	192	132	148
dx_{ELDOR} (ns)	8	8	8	8
No. of points	160	156	160	160

u: without maltose; l: with maltose

Table A 7. Parameters for CW measurement (MBP8)

MBP8	pH 3, u	pH 3, l	pH 7, u	pH 7, l
Field center (G)	3480	3480	3480	3480
Field width (G)	200	200	200	200

Averaged scans	20	20	20	20
Sampling time (s)	0.02048	0.02048	0.02048	0.02048
Field modulation amplitude (T)	0.0001	0.0001	0.0001	0.0001
Field modulation frequency (Hz)	100000	100000	100000	100000
Microwave frequency (GHz)	9.781	9.778	9.782	9.778
Microwave power (W)	$6.377*10^{-5}$	$6.377*10^{-5}$	$6.377*10^{-5}$	$6.392*10^{-5}$
Receiver gain	60	60	60	60
Receiver time constant (s)	0.00128	0.00128	0.00128	0.00128
Receiver phase (deg)	0.0	0.0	0.0	0.0
Receiver harmonic	1	1	1	1
Receiver offset (%FS)	0.0	0.0	0.0	0.0

u: without maltose; l: with maltose

Table A 8. Parameters for CW measurement (MBP12)

MBP12	pH 3, u	pH 3, l	pH 7, u	pH 7, l
Field center (G)	3472	3472	3474	3474
Field width (G)	150	150	150	150
Averaged scans	10	10	10	10
Sampling time (s)	0.04096	0.04096	0.04096	0.04096
Field modulation amplitude (T)	0.0001	0.0001	0.0001	0.0001
Field modulation frequency (Hz)	100000	100000	100000	100000
Microwave frequency (GHz)	9.768	9.769	9.769	9.771
Microwave power (W)	$6.377*10^{-5}$	$6.377*10^{-5}$	$6.377*10^{-5}$	$6.377*10^{-5}$
Receiver gain	40	40	40	40
Receiver time constant (s)	0.01024	0.01024	0.01024	0.01024
Receiver phase (deg)	0.0	0.0	0.0	0.0
Receiver harmonic	1	1	1	1
Receiver offset (%FS)	0.0	0.0	0.0	0.0

u: without maltose; l: with maltose

VII. ACKNOWLEGEMENT

I would like to express my special gratitude to my supervisor Professor Trommer for giving me the opportunity to work on this very interesting project. I appreciate his kind guidance, necessary encouragement and useful comments.

I would like to acknowledge our cooperative labs. Professor Freed and Dr. Borbat from ACERT National Biomedical Center for Advanced ESR Technology, Cornell University, USA, offered the opportunity to carry out the DQC measurements. Professor Keller from Molecular Physik, TU Kaiserslautern, was very kind to provide ITC200 and CD spectrometer for my measurements. He and his co-workers helped me to carry out the experiment and analyze the data. I am very grateful. Professor Niedner-Schatteburg from Physikalische Chemie, TU Kaiserslautern, was also very kind to provide the MALDI-TOF MS. I am grateful that I could always get answers from his work group, whenever I had questions. Professor Varadarajan from Molecular Biophysics Unit, Indian Institute of Science, India, provided plasmids of the double mutants MBP1 to MBP7 and Professor Hideg from University of Pécs, Hungary, provided spin labels MTS, so that this project could have been started up. I appreciate that.

I would like to thank Professor Keller and Dr. Philipp especially for their precious time to review my paperwork. I would like to thank Professor Pierik for sharing his knowledge on gene technology, chromatography and EPR. I would like to thank Dr. Netz as well for her kind guidance on mutagenesis and cloning. I would not forget to thank Jörg Reichenwallner and Anna Weyrauch for helping me with the pulsed EPR experiment.

I am very grateful to work with my colleagues at the work group of Professor Trommer and the colleagues from the cooperative labs. They shared their experience with me and gave me their

opinions and suggestions. They supported me physically and mentally. I am grateful for the unforgettable time.

I would also like to thank Ms Fluck for her kind help anytime when I came to her.

Also I would like to give my gratitude to my friends. They were always open to give me their opinions, although they worked on the different majors. I enjoyed the time to discuss with them, so that I could find out the answers in different ways. I would like to thank Jonathan Meyer, Kai Pfister and Tobias Pfeiffer for their precious time to give comments to my paperwork.

At last I would like to give my profound gratitude to my family, who always supported me during the whole study time. My parents give me the opportunity to start my study in Germany and help me to deal with the problems whatever I met. My husband Patrick supports me without complaint especially during the tough time. Without them I would have not finished my degree.

The all experience and the precious time will stay in my memory. Thank you all for making it happen.

Ph. D. Studies:

05/2013	Beginning of Ph. D. Studies at Department of Chemistry/ Biochemistry, Technical University of Kaiserslautern Under supervision of Prof. Dr. Wolfgang E. Trommer Thesis: The Molten Globule State of Maltose-Binding Protein: Structural Characterization by Electron Paramagnetic Resonance Spectroscopy

Kaiserslautern, den 22.10.2016 Chen Nickolaus